Ligand Substituent, Anion, and Solvation Effects on Ion Pair Structure, Thermodynamic Stability, and Structural Mobility in "Constrained Geometry" Olefin Polymerization Catalysts: an Ab Initio Quantum Chemical Investigation

Giuseppe Lanza,*,† Ignazio L. Fragalà,*,‡ and Tobin J. Marks*,§

Contribution from the Department of Chemistry, Northwestern University, 2145 Sheridan Road, Evanston Illinois 60208-3113

Received February 16, 2000. Revised Manuscript Received August 31, 2000

Abstract: Ab initio quantum chemical calculations at the MP2 level were performed on the elementary reactions and structural reorganizations involved in activation and ligand binding by the "constrained geometry" olefin polymerization catalyst series $R_2Si(\eta^5\text{-}R'_4C_5)(R''N)Ti(CH_3)R'''$ (R = H, CH_3; R′ = H, CH_3; R″ = CH_3, *t*-Bu; R‴ = H, CH_3, $CH_2CH_2CH_3$, $CH(CH_3)_2$) in the presence of the organo-Lewis acid cocatalyst $B(C_6F_5)_3$ and various solvation media. Calculated structures of the neutral precursors and resulting ion pairs are in good agreement with the experiment. Analysis of the $R_2Si(R'_4C_5)(R''N)TiR'''^+$ naked cations reveals the importance of α, *β*, and *γ* C−H/C−C agostic interactions in selectively stabilizing various conformations of the TiR‴ group as well as the diminished charge on Ti with the introduction of electron-donating ligand substituents. The calculated ion pair formation enthalpies for the process $R_2Si(\eta^5\text{-}R'_4C_5)(R''N)Ti(CH_3)R''' + B(C_6F_5)_3 \rightarrow R_2Si(\eta^5\text{-}R'_4C_5)(R''N)TiR'''\cdot H_3CB(C_6F_5)_3$ are in good agreement with experiment, the magnitudes reflecting a close interplay of ligand electronic and steric characteristics which weaken the precursor Ti−CH_3 bond and stabilize the cationic product. The ion pair Ti···H_3CB interaction is predominantly electrostatic in character and describable by a rather flat potential energy surface for elongation, and the energetics of heterolysis are strongly influenced by the capacity of the other Ti ligands and solvation to stabilize the separated charges.

Introduction

The discovery of structurally well-defined single-site catalysts for olefin polymerization has stimulated intense academic and industrial research activity focused on understanding structure−reactivity−selectivity relationships as well as on enhancing the properties of the derived polymeric products.[1] Increasingly, polymer tacticity, molecular weight, comonomer incorporation, and long chain branching can be tuned to a significant extent by suitable modulation of both the catalyst and cocatalyst architectures.[1] In this context, single-site "constrained geometry catalysts" (CGC; e.g., **A**, eq 1) have provided significant

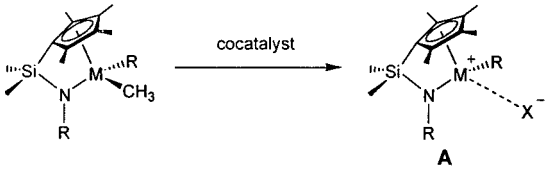

(1)

A

advances in affording polymeric materials with unprecedented control over macromolecular architecture; superior polymer processing/mechanical properties due to the narrow molecular weight distribution, combined with long chain branching; and high degrees of comonomer incorporation.[1e,2] Moreover, the replacement of a metallocene cyclopentadienyl ring with a simple alkylamido group favors polymerization of long-chain α-olefins and ethylene copolymerization with heretofore impossible, sterically encumbered comonomers, presumably connected

† Dipartimento di Chimica, Università della Basilicata, 85100 Potenza, Italy.

‡ Dipartimento di Scienze Chimiche, Università di Catania, 95125 Catania, Italy.

§ Northwestern University

(1) For recent reviews, see: (a) Chen, E. Y.-X.; Marks, T. J. *Chem. Rev.* **2000**, *100*, 1391. (b) Marks, T. J., Stevens, J. C., Eds. *Top. Catal.* **1999**, *7*, 1 (special volume on "Advances in Polymerization Catalysis. Catalysts and Processes"). (c) Kaminsky, W. *Metalorganic Catalysts for Synthesis and Polymerization: Recent Results by Ziegler−Natta and Metallocene Investigations*; Springer−Verlag: Berlin, 1999. (d) Britovsek, G. J. P.; Gibson, V. C.; Wass, D. F. *Angew. Chem., Int. Ed. Engl.* **1999**, *38*, 428 (nonmetallocene olefin polymerization catalysts). (e) Jordan, R. F. *J. Mol. Catal.* **1998**, *128*, 1 (special issue on metallocene and single-site olefin catalysts). (f) McKnight, A. L.; Waymouth, R. M. *Chem. Rev.* **1998**, *98*, 2587 (constrained geometry polymerization catalysts). (g) Kaminsky, W.; Arndt, M. *Adv. Polym. Sci.* **1997**, *127*, 144. (h) Bochmann, M. *J. Chem. Soc., Dalton Trans.* **1996**, 255. (i)Brintzinger, H. H.; Fischer, D.; Mülhaupt, R.; Rieger, B.; Waymouth, R. M. *Angew. Chem., Int. Ed. Engl.* **1995**, *34*, 1143−1170. (j) Soga, K.; Teramo, M. *Catalyst Design for Tailor-Made Polyolefins*; Elsevier: Amsterdam, 1994.

(2) (a) Brown, S. J.; Gao, X.; Harrison, D. G.; Koch, L.; Spence, R. E. H.; Yap, G. P. A. *Organometallics* **1998**, *17*, 5445. (b) McKnight, A. L.; Masood, M. A.; Waymouth, R. M.; Straus, D. A. *Organometallics* **1997**, *16*, 2879. (c) Chen, Y. X.; Marks, T. J. *Organometallics* **1997**, *16*, 3649. (d) Carpenetti, D. W.; Kloppenbrug, L.; Kupec, J. T.; Petersen, J. L. *Organometallics* **1996**, *15*, 1572. (e) Stevens, J. C. In *Studies in Surface Science and Catalysis*; Hightower, J. W., Delglass, W. N., Iglesia, E., Bell, A. T., Eds.; Elsevier: Amsterdam, 1996, Vol. 101; p. 11, and references therein. (f) Stevens, J. C. In *Catalyst Design for Tailor-Made Polyolefins*, Elsevier: Amsterdam, 1994; p 277. (g) Devore, D. D.; Timmers, F. J.; Hasha, D. L.; Rosen, R. K.; Marks, T. J.; Deck, P. A.; Stern, C. L. *Organometallics* **1995**, *14*, 3132. (h) Stevens, J. C.; Timmers, F. J.; Wilson, D. R.; Schmidt, G. F.; Nickias, P. N.; Rosen, R. K.; Knight, G. W.; Lai, S. European Patent Application EP-416-815-A2, March 13, 1991. (i) Canich, J. A. PCT Application WO 91/04257, April, 4, 1991. (j) Shapiro, P. J.; Bunel, E.; Schaefer, W. P.; Bercaw, J. E. *Organometallics* **1990**, *9*, 867.

10.1021/ja000571r CCC: $19.00
Published on Web 12/05/2000

with enhanced coordinative unsaturation and reduced steric crowding at the metal center.[2]

Recent theoretical studies have provided invaluable insight into many mechanistic aspects of metallocenium catalytic processes.[3−5] Nevertheless, they have largely employed a "naked cation" description in which solvation and the counteranion are not explicitly considered. However, growing experimental evidence now suggests that cation−cocatalyst counteranion interactions and solvation can play a significant role in ion pairing energetics as well as in catalytic activity and selectivity and in ways that are not well-understood.[1,6−8] Thus, there are data arguing that the polymerization rate, enchainment stereospecificity, product molecular weight, and catalyst stability depend significantly upon catalyst and cocatalyst structure, as well as on the reaction solvent. In the case of ethylene polymerization processes, it has also been reported, counter to intuition, that electron-donating substituents on the catalyst ancillary ligands lead to enhanced catalytic activity, whereas electron-withdrawing substituents have the opposite effect.[1]

The above considerations raise intriguing questions concerning the ion pair equilibria operative in formation processes for, and in the reaction patterns of, the cation-like species which are the active catalysts. In a preliminary communication,[9] we reported the first ab initio theoretical evidence that the energetics of counteranion and solvation sphere interactions with a model cationic catalytic center are significant and that they strongly affect the pathway of olefin activation and insertion. The results argue that any realistic modeling of single-site catalysts must go beyond the naked cation approach. In the present contribution, we report a full account of our theoretical analyses at the ab initio SCF and MP2 levels, focusing on the formation and reactivity of a family of $R_2Si(\eta^5\text{-}R'_4C_5)(R''N)TiR'''^+$ catalysts, including anion and solvation effects. We explore in detail the energetics associated with the methide abstraction/catalyst activation process to form contact ion pairs (eq 2), the energetics

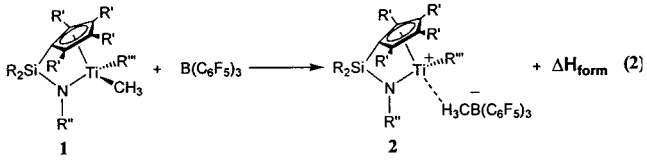

1 2

of heterolytic ion-pair separation relevant to the "tightness" of the ion pairing (eq 3), and the effects of solvation on the naked

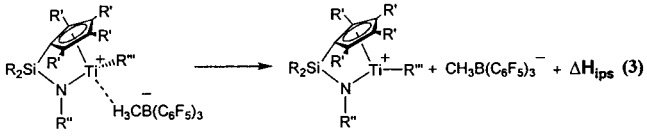

2 3

R = H, CH_3 R' = H, CH_3 R'' = CH_3, $C(CH_3)_3$

R''' = H, CH_3, $CH_2CH_2CH_3$, $CH(CH_3)_2$

cation (eq 4) using various Ti−CGC ligation array models.

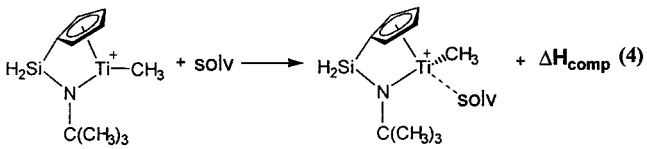

solv = C_6H_6, C_6H_5Cl, CH_2Cl_2

Included are calculations for a "real-world" catalyst, $(CH_3)_2Si[(CH_3)_4C_5)](t\text{-}BuN)Ti(CH_3)_2$, combined with a real-world cocatalyst, $B(C_6F_5)_3$.[1,2,6] Importantly, a selected range of model molecules having differing substituents on the amido and cyclopentadienyl ligands, as well as having different Ti-alkyl groups (to simulate a growing polymer chain), are included in the analysis.

Two sets of model systems have been considered: (i) structures having identical metal alkyl groups but with varying ancillary ligand substituents (**1a**, **d**), and (ii) systems with identical ancillary ligation but with varying metal-bound alkyl groups (**1c**,**e**−**g**). The breadth of this investigation allows detailed analysis of the energetics of eqs 2−4 and how they depend on ancillary ligand donor characteristics, fluoroarylborate counteranion positioning, Ti−alkyl agostic interactions, and finally, solvation. Some aspects of ancillary ligand substituent and solvation effects in analogous systems have been recently reported in complementary studies by Ziegler et al. using a density functional (DFT) approach.[5a,b] Where appropriate, comparison to the present results will be of interest. Several other recent DFT studies have investigated related types of

(3) (a) Yoshida, T.; Koga, N.; Morokuma, K. *Organometallics* **1996**, *15*, 766. (b) Yoshida, T.; Koga, N.; Morokuma, K. *Organometallics* **1995**, *14*, 746. (c) Weiss, H.; Ehrig, M.; Ahlrichs, R. *J. Am. Chem. Soc.* **1994**, *116*, 4919. (d) Bierwagen, E. P.; Bercaw, J. E.; Goddard III, W. A. *J. Am. Chem. Soc.* **1994**, *116*, 1481. (e) Kawamura-Kuribayashi, H.; Koga, N.; Morokuma, K. *J. Am. Chem. Soc.* **1992**, *114*, 8687.

(4) (a) Margl, P. M.; Woo, T. K.; Blöchl, P. E.; Ziegler, T. *J. Am. Chem. Soc.* **1998**, *120*, 2174. (b) Woo, T. K.; Margl, P. M.; Ziegler, T.; Blöchl, P. E. *Organometallics* **1997**, *16*, 3454. (c) Woo, T. K.; Margl, P. M.; Lohrenz, J. C. W.; Blöchl, P. E.; Ziegler, T. *J. Am. Chem. Soc.* **1996**, *118*, 13021. (d) Margl, P. M.; Lohrenz, J. C. W.; Ziegler, T.; Blöchl, P. E. *J. Am. Chem. Soc.* **1996**, *118*, 4434. (e) Lohrenz, J. C. W.; Woo, T. K.; Ziegler, T. *J. Am. Chem. Soc.* **1995**, *117*, 12793. (f) Fan, L.; Harrison, D.; Woo, T. K.; Ziegler, T. *Organometallics* **1995**, *14*, 2018. (g) Meier, R. J.; Doremaele, G. H. J. V.; Iarlori, S.; Buda, F. *J. Am. Chem. Soc.* **1994**, *116*, 7274. (h) Woo, T. K.; Fan, L.; Ziegler, T. *Organometallics* **1994**, *13*, 2252. (i) Woo, T. K.; Fan, L.; Ziegler, T. *Organometallics* **1994**, *13*, 432.

(5) To our knowledge, the only other metallocenium studies (DFT) to include the anion are the following: (a) Vanka, K.; Chan, M. S. W.; Pye, C.; Ziegler, T. *Organometallics* **2000**, *19*, 1841. (b) Chan, M. S. W.; Vanka, K.; Pye, C. C.; Ziegler, T. *Organometallics* **1999**, *18*, 4624. (c) Klesing, A.; Bettonville, S. *Chem. Phys. Phys. Chem.* **1999**, *1*, 2373. (d) Yakota, Y.; Inoue, T.; Nagamura, S.; Shozaki, H.; Tomotsu, N.; Kuramoto, M.; Ishihara, N. In *Metalorganic Catalysts for Synthesis and Polymerization: Recent Results by Ziegler−Natta and Metallocene Investigations*; Springer−Verlag: Berlin, 1999; p 435. (e) Fusco, R.; Longo, L.; Masi, F.; Garbasi, F. *Macromol. Rapid Commun.* **1997**, *18*, 433. (f) Fusco, R.; Longo, L.; Masi, F.; Garbasi, F. *Macromolecules* **1997**, *30*, 7673. (g) Fusco, R.; Longo, L.; Proto, A.; Masi, F.; Garbasi, F. *Macromol. Rapid Commun.* **1998**, *19*, 257.

(6) (a) Beswick, C. L.; Marks, T. J. *J. Am. Chem. Soc.* **2000**, *122*, 10358. (b) Beswick, C. L.; Marks, T. J. *Organometallics* **1999**, *18*, 2410. (c) Chen, Y.-X.; Metz, M. V.; Li, L.; Stern, C. L.; Marks, T. J. *J. Am. Chem.* **1998**, *120*, 6287. (d) Marks, T. J.; Stevens, J. C., Eds. *Top. Catal.* **1999**, *7*, 45. (e) Deck, P. A.; Beswick, C. L.; Marks, T. J. *J. Am. Chem. Soc.* **1998**, *120*, 1772. (f) Chen, Y.-X.; Stern, C. L.; Marks, T. J. *J. Am. Chem.* **1997**, *119*, 2582. (g) Jia, L.; Yang, X.; Stern, C. L.; Marks, T. J. *Organometallics* **1997**, *16*, 842. (h) Chen, Y.-X.; Stern, C. L.; Yang, S. T.; Marks, T. J. *J. Am. Chem. Soc.* **1996**, *118*, 12451. (i) Giardello, M. A.; Eisen, M. S.; Stern, C. L.; Marks T. J. *J. Am. Chem. Soc.* **1995**, *117*, 12114. (j) Deck, P. A.; Marks, T. J. *J. Am. Chem. Soc.* **1995**, *117*, 6128. (k) Yang, X.; Stern, C. L.; Marks, T. J. *J. Am. Chem. Soc.* **1994**, *116*, 10015.

(7) (a) Shiomura, T.; Asanuma, T.; Inoue, N. *Macromol. Rapid Commun.* **1996**, *17*, 9. (b) Soga, K.; Teramo, M. *Catalyst Design for Tailor-Made Polyolefins*; Elsevier: Amsterdam, 1994; p 221.

(8) (a) Feichtinger, D.; Plattner, D. A.; Chen, P. *J. Am. Chem. Soc.* **1998**, *120*, 7125. (b) Richardson, D. E.; Alameddin, N. G.; Ryan, M. F.; Hayes, T.; Eyler, J. R.; Siedle, A. R. *J. Am. Chem. Soc.* **1996**, *118*, 11244. (c) Alameddin, N. G.; Ryan, M. F.; Eyler, J. R.; Siedle, A. R.; Richardson, D. E. *Organometallics* **1995**, *14*, 5005.

(9) (a) Lanza, G.; Fragalà, I. L.; Marks, T. J. *J. Am. Chem. Soc.* **1998**, *120*, 8257. (b) Lanza, G.; Fragalà, I. L. In *Topics in Catalysis*; Marks, T. J., Stevens, J. C., Eds., **1999**, *7*, p 45 (special volume on "Advances in Polymerization Catalysis. Catalysts and Processes").

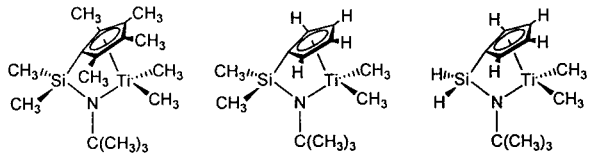

1a

1b

1c

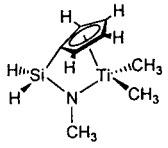

1d

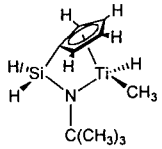

1e

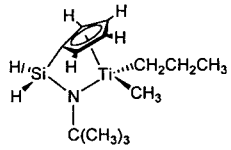

1f

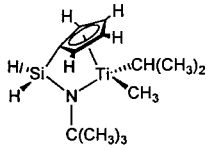

1g

cation−anion pairs.[5c−f] The purpose of the present contribution is to best understand structure, bonding, and bond making/bond breaking in real-world catalysts with elaborate real-world ligation as well as with the all-important, tightly ion-paired cocatalyst counteranion and the solvation medium. This is clearly a daunting computational challenge. It is beyond the scope of this contribution to discuss the relative merits of ab initio versus DFT techniques when applied to such problems; however, note that realistic treatments of electron correlation will undoubtedly be important in modeling catalyst structures along reaction coordinates that are far from equilibrium and in obtaining an accurate orbital picture of the bonding. There are situations in which DFT techniques may be limited in their ability to model partially bonded nonequilibrium structures or differentiate between isomers of similar energy, or may be overly sensitive to choice of exchange potentials.[10] Here, ab initio methods should be advantageous in accounting explicitly for evaluation of nonlocal exchange integrals. Dealing with the present real-world catalyst systems necessarily precludes the use of extremely large basis sets or including correlation beyond MP2. Nevertheless, the MP2 treatment acts uniformly on each of the points on a potential energy surface, and while absolute quantification of correlation energies may not be possible, relative trends offset by a scaling factor should be reliable. This will be tested herein versus a large experimental database.

Computational Details

The effective core potentials (ECP) of Hay and Wadt,[11a] which explicitly treat 3s and 3p electrons and a basis set contracted as [3s3p2d], were used for the Ti atom. The standard all-electron 6-31G basis was used for the remaining atoms.[11b,c] Geometry optimization used analytical gradient techniques within the restricted Hartree−Fock (HF) formalism. Correlation effects were evaluated adopting MP2 wave functions where all valence electrons, including the titanium 3s and 3p, are correlated. The basis set superposition error (BSSE) was estimated by the counterpoise method.[12] As noted in the Introduction, the goal of this study was to assess trends in cationic catalyst architecture, energetics, and bonding with the perfluoroarylborate counteranion and solvation included; that is, to attempt for the first time to model the actual catalyst system in solution at the ab initio level. This represents a nontrivial computational undertaking (e.g., complex **2a** consists of 87 atoms, is described by 571 basis functions and 1383 primitive Gaussians, and has no symmetry elements), and although more elaborate calculations would certainly be desirable, they are beyond the capacities of most computational groups and are not expected to increase the accuracy greatly. Nevertheless, some test calculations, including d polarization functions on C, N, Si, B, and Cl atoms, were performed in order to check the reliability of the adopted basis set (MP2 calculations with up to 628 basis functions and 1287 primitive Gaussians were performed). As will be seen, the results are not significantly affected by polarization function inclusion, and certainly the double-ζ quality basis set presently used represents a good compromise between feasibility and calculational accuracy. An important aspect of the present calculations is associated with the BSSE correction. The inclusion of polarization functions has a modest effect on BSSE, and only the use of very large basis sets (several thousands of basis functions) would reduce its magnitude. This trend is in agreement with the results of several recent studies showing that as the basis set is improved systematically, the BSSE correction decreases only minimally, and the addition of a polarization function (hence, the 6-31G** basis set) results in only minor diminution in the BSSE.[13]

Solvent effects were modeled using the self-consistent isodensity polarized continuum formalism (SCI−PCM). The SCI−PCM method models the solvent as a continuum of uniform dielectric constants, and the solute is placed into a cavity within the solvent. The cavity is defined as an isodensity surface and is coupled with the electron density of the solute. In this method, the effects of solvation are folded into the iterative SCF procedure.[14a−c] An electron density cutoff of $\rho = 0.0004$ was used to determine the solute boundary for the SCI−PCM calculations. The dielectric constants of the solvents investigated are C_6H_6, 2.274; C_6H_5Cl, 5.71; and CH_2Cl_2, 9.08.

All of the calculations were performed using the HONDO 95.3 and G94 codes[14c,d] on IBM-SP and Origin 2000 systems.

Results and Discussion

This section begins with a discussion of the computed structures and bonding in the neutral dialkyl precatalysts and compares them to experimental X-ray diffraction data. These results are then compared and contrasted to those for the naked monoakyl cations prepared by abstraction of an alkyl anion. The importance of ancillary ligand steric and electronic effects and agostic interactions is assessed. Next, the neutral dialkyls are activated with the organo-Lewis acid cocatalyst $B(C_6F_5)_3$ to yield catalytically active contact cation−anion pairs. The

(10) (a) Raghavachari, K.; Anderson, J. B. *J. Phys. Chem.* **1996**, *100*, 12960. (b) Head-Gordon, M. *J. Phys. Chem.* **1996**, *100*, 13213. (c) Ziegler, T. *Chem. Rev.* **1991**, *91*, 651 and references therein. (d) Jensen, F. *Introduction to Modern Computational Chemistry*; Wiley: New York, 1999.

(11) (a) Hay, P. J.; Wadt, W. R. *J. Chem. Phys.* **1985**, *82*, 299. (b) Hehre, W. J.; Ditchfield, R.; Pople, J. A. *J. Chem. Phys.* **1972**, *56*, 2257. (c) Franel, M. M.; Pietro, W. J.; Hehre, W. J.; Binkley, J. S.; Gordon, M. S.; DeFrees, D. J.; Pople, J. A. *J. Chem. Phys.* **1982**, *77*, 3654.

(12) Boys, S. F.; Bernardi, F. *Mol. Phys.* **1970**, *19*, 553.

(13) (a) Pelmenschikov, A.; Leszczynskin, J. *J. Phys. Chem. B* **1999**, *103*, 6886. Less than 1 kcal/mol variation in BSSE correction is observed for the calculated interaction energy of 1,3,5-trinitrobenzene and a siloxane surface at the 6-31G, 6-31+G, 6-31G*, 6-311G , and 6-311G* levels. (b) Halkier, A.; Koch, H.; Jorgensen, P.; Christiansen, O.; Nielsen, I. M. B.; Helgaker, T. *Theor. Chim. Acta* **1997**, *97*, 150. The interaction energy of the water dimer is reported to stabilize at the MP2 level when an aug-cc-pV5Z basis set is used (574 basis functions). (c) Machado, F. B. C.; Davidson, E. R. *J. Phys. Chem.* **1993**, *97*, 4397. For the formation energy of $Cr(CO)_6$, a BSSE correction of 32.8 kcal/mol is observed with a very large basis set (close to the HF limit) at the MP2 level.

(14) (a) Foresman, J. B.; Keith, T. A.; Wiberg, K. B.; Snoonian, J.; Frisch, M. J. *J. Phys. Chem.* **1996**, *100*, 16098. (b) Foresman, J. B.; Frisch, E. *Exploring Chemistry with Electronic Structure Methods*, Gaussian Inc.: Pittsburgh, PA, 1996. (c) Frisch, M. J.; Trucks, G. W.; Schlegel, H. B.; Gill, P. M. W.; Johnson, B. G.; Robb, M. A.; Cheeseman, J. R.; Keith, T. A.; Petersson, G. A.; Montgomery, J. A.; Raghavachari, K.; Al-Laham, M. A.; Zakrzewski, V. G.; Ortiz, J. V.; Foresman, J. B.; Cioslowski, J.; Stefanov, B. B.; Nanayakkara, A.; Challcombe, M.; Peng, C. J.; Ayala, P. Y.; Chen, W.; Wong, M. W.; Andres, J. L.; Replogle, E. E. S.; Gomperts, R.; Martin, R. L.; Fox, D. J.; Binkley, J. S.; Defrees, D. J.; Baker, J.; Stewart, J. P.; Head-Gordon, M.; Gonzalez, C.; Pople, J. A. Gaussian-94; Gaussian Inc.: Pittsburgh, PA, 1995. (d) Dupuis, M.; Marquez, A.; Davidson, E. R. HONDO 95.3 from CHEM-Station.; IBM Corporation: Kingston, NY, 1995.

Table 1. Computed HF and Experimental Bond Lengths (Å) and Angles (deg) of Neutral Constrained-Geometry $R_2Si(\eta^5\text{-}R'_4C_5)(R''N)Ti(CH_3)R'''$ Dialkyl/Hydridoalkyl Precatalysts (1)[a]

	1a R = R′ = R‴ = CH_3 R″ = *t*-Bu	**1b** R = R‴ = CH_3 R′ = H R″ = *t*-Bu	**1c** R = R′ = H R″ = *t*-Bu R‴ = CH_3	**1d** R = R′ = H R″ = R‴ = CH_3	**1e** R = R′ = R‴ = H R″ = *t*-Bu	**1f** R = R′ = H R″ = *t*-Bu R‴ = *n*-Pr	**1g** R = R′ = H R″ = *t*-Bu R‴ = *i*-Pr
			Bond Lengths[b]				
Ti−C(1) Ti−C(2)	2.092 (2.087(7))	2.086	2.080	2.077	1.658, 2.075	2.086 (2.081)	2.125 (2.079)
Ti−Cp centroid	2.142 (2.061)	2.175	2.181	2.165	2.152	2.187	2.194
Ti−N	1.936 (1.957(7))	1.923	1.919	1.899	1.907	1.920	1.926
N−Si	1.816 (1.693(7))	1.823	1.811	1.794	1.810	1.807	1.809
Si−C(3)	1.906 (1.851(7))	1.890	1.883	1.889	1.888	1.884	1.881
C(1)−H(1)	1.088 (0.950)	1.086	1.086	1.089		1.091	1.094
C(1)−H(2)	1.088 (0.947)	1.088	1.088	1.088		1.091	(1.542)[c]
C(1)−H(3)	1.091 (0.950)	1.087	1.087	1.088		(1.537)[d]	(1.541)[d]
			Bond Angles[b]				
C(1)−Ti−C(2)	98.3 (102.4(4))	96.9	98.4	102.7	97.3	98.1	97.2
Θ[e]	49.2 (48.5)	48.5	49.2	51.3	57.9	49.6	40.7
N−Ti−Cp centroid	108.8 (115.5)	108.1	108.3	106.0	108.5	107.8	107.3
Ti−N−Si	103.2 (100.7(3))	103.4	102.9	105.4	103.3	103.3	103.3
N−Si−C(3)	91.7 (94.6(3))	92.1	93.4	92.1	92.8	93.4	93.5
Ti−C(1)−H(1)	110.0 (109.4)	110.8	110.4	110.3		105.0	99.3
Ti−C(1)−H(2)	110.9 (109.5)	110.0	110.6	110.5		107.2	(114.3)[f]
Ti−C(1)−H(3)	111.5 (109.2)	111.2	110.8	110.7		(118.6)[g]	(118.0)[g]

[a] Experimental data from refs 2g and 15 in parentheses. [b] Atom labeling defined in Figure 1. [c] C(1)−C(9) bond length. [d] C(1)−C(8) bond length. [e] Angle between the Cp centroid-Ti−N plane and the Ti−C(1) vector. [f] Ti−C(1)−C(9) bond angle. [g] Ti−C(1)−C(8) bond angle.

geometries and electronic structures of the ion pairs are analyzed as a function of metal ligation and compared to experiment (X-ray diffraction). Then energetics of this process are analyzed as a function of ancillary ligation and solvation and are compared to experiment (solution reaction calorimetry; NMR equilibration measurements). The energetics of heterolytic ion pair separation processes are next scrutinized, and the effects of various ligand and solvent environments are assessed and compared to experiment (dynamic NMR spectroscopy). The energetics of solvated naked cations and the possible role of discrete solvent complexes is then explored. Finally, the computational information is used in combination with experimental data to analyze the components of a Born−Haber cycle that describes the thermochemistry of ion pair formation and separation.

Molecular Structures of the $R_2Si(\eta^5\text{-}R'_4C_5)(R''N)Ti(CH_3)R'''$ Precatalysts. Figure 1 shows schematic representations of several computed precatalyst (**1**) structures, while Table 1 collects significant metrical parameters and compares them to the available experimental data.[15] Considering the complexity of the calculations, there is good agreement between the computed and experimental[15] metrical parameters. The Ti centers in all precatalyst molecules have pseudotetrahedral arrangements, and complexes with identical Ti−alkyl substituents (R‴ = CH_3) possess rigorous C_s symmetry. In the cases of nonidentical alkyl groups (R‴ = H, C_3H_7), the $R_2Si(R'_4C_5)(R''N)Ti<$ fragment still possesses approximate local C_s symmetry, with the symmetry plane through the Ti, N, and Si atoms bisecting the Cp ring and the C(1)−Ti−C(2) angle [the C(1)−Ti−C(2) angle is approximately 2 Θ, the angle between the Cp (centroid)-Ti−N plane and the Ti−C(1) vector; Table 1]. In the case of the *n*-propyl- and isopropyl-Ti derivatives, the alkyl groups assume conformations which minimize interligand repulsive interactions, with the alkyl chains disposed far from the Ti and other ligands. Various conformers of the *n*-propyl derivative, related by rotation about the Ti−C and/or C−C bonds, lie close in energy (ΔE < 1 kcal/mol); only one computed conformation is shown in Figure 1. Varying the R (Si), R′ (ring), and R″ (N) substituents induces minor structural alterations; namely, some lengthening of bond distances is observed which parallels the increasing electron donor character of the R, R′, and R″ substituents. This observation agrees well

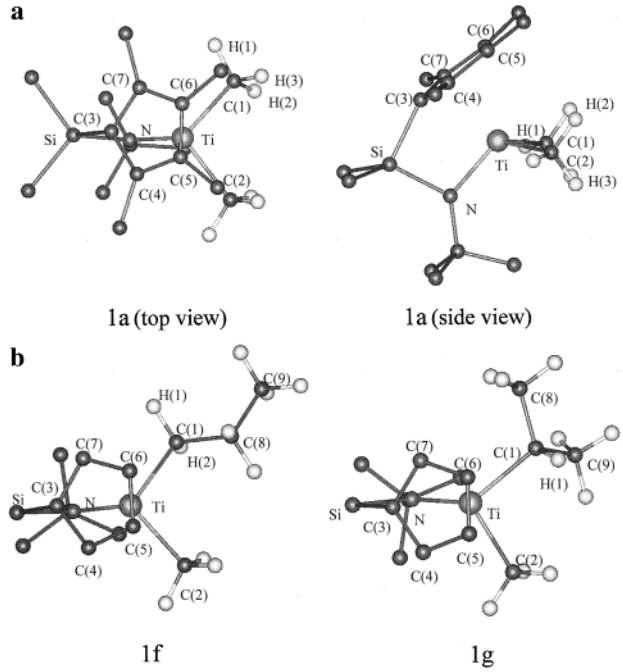

Figure 1. Molecular structures of selected precatalysts: **1a**, $(CH_3)_2Si[(CH_3)_4C_5](t\text{-}BuN)Ti(CH_3)_2$ (top and side views); **1f**, $H_2Si(C_5H_4)(t\text{-}BuN)Ti(CH_3)(CH_2CH_2CH_3)$; and **1g**, $H_2Si(C_5H_4)(t\text{-}BuN)Ti(CH_3)[(CH(CH_3)_2)]$. Hydrogen atoms on the $R_2Si(C_5R'_4)(R''N)$ ligand have been omitted for clarity.

(15) (a) Fu, P.-F.; Lanza, G.; Wilson, D. J.; Rudolph, P. R.; Fragalà, I. L.; Stern, C. L.; Marks, T. J. Manuscript in preparation. (b) **1a** crystallographic data: space group *Pnma* (#62); a = 12.253(1) Å, b = 13.467(1) Å, c = 11.892(3) Å; Z = 4. Structure was solved by direct methods and refined using weighted and unweighted difference Fourier syntheses and full-matrix least-squares. R_F = 0.050, wR_F = 0.046 for 2013 absorption-corrected reflections with I > 3.0 σ(I). (c) **2a** crystallographic data: space group P1 (#2); a = 9.178(3) Å, b = 12.031(2) Å, c = 17.218(4) Å, α = 78.39(2)°, β = 76.17(2) °, γ = 78.98(2) °; Z = 2. Structure was solved by direct methods and refined using weighted and unweighted difference Fourier syntheses and full-matrix least-squares. R_F = 0.041, wR_F = 0.043 for 4418 absorption-corrected reflections with I > 3 σ(I).

Table 2. HF Bond Lengths (Å) and Bond Angles (deg) in Naked $R_2Si(\eta^5\text{-}R'_4C_5)(R''N)TiR'''^+$ Constrained Geometry Cations (3).

	3a R = R′ = R‴ = CH_3, R″ = *t*-Bu	**3b** R = R‴ = CH_3, R′ = H, R″ = *t*-Bu	**3c** R = R′ = H, R″ = *t*-Bu, R‴ = CH_3	**3d** R = R′ = H, R″ = R‴ = CH_3	**3e** R = R′ = R‴ = H, R″ = *t*-Bu	**3f** R = R′ = H, R″ = *t*-Bu, R‴ = *n*-Pr	**3g** R = R′ = H, R″ = *t*-Bu, R‴ = *i*-Pr
			Bond Lengths[a]				
Ti−C(1)	2.058	2.043	2.033	2.026	(1.636)	2.022	2.016
Ti−Cp centroid	2.031	2.064	2.071	2.070	2.048	2.081	2.080
Ti−N	1.858	1.838	1.838	1.828	1.827	1.849	1.851
N−Si	1.853	1.877	1.855	1.848	1.837	1.844	1.847
Si−C(3)	1.932	1.911	1.900	1.904	1.908	1.899	1.901
C(1)−H(1)	1.092	1.092	1.092	1.093		1.085	1.091
C(1)−H(2)	1.092	1.092	1.092	1.093		1.078	(1.542)[b]
C(1)−H(3)	1.083	1.082	1.083	1.084		(1.536)[c]	(1.524)[c]
			Bond Angles[a]				
Θ[d]	0.0	0.0	0.0	0.0	43.2	19.2	13.5
N−Ti−Cp centroid	112.2	111.9	111.4	110.2	110.3	111.3	111.9
Ti−N−Si	103.9	103.8	103.6	105.3	105.8	103.3	102.7
N−Si−C(3)	88.9	88.6	89.9	89.3	88.1	90.3	90.7
Ti−C(1)−H(1)	109.4	109.2	108.9	108.8		111.1	87.6
Ti−C(1)−H(2)	109.4	109.2	108.9	108.8		111.8	(103.2)[e]
Ti−C(1)−H(3)	115.8	115.3	115.9	116.0		(88.4)[f]	(128.5)[f]

[a] Atom labeling defined in Figure 2. [b] C(1)−C(9) bond length. [c] C(1)−C(8) bond length. [d] Angle between the Cp centroid-Ti−N plane and the Ti−C(1) vector. [e] Ti−C(1)−C(9) bond angle. [f] Ti−C(1)−C(8) bond angle.

with the greater expected molar volumes; hence, greater delocalization of electron density and greater interligand nonbonded repulsion (with consequent bond weakening) incurred upon replacement of H atoms with either CH_3 or larger alkyl groups. The same trend has been found in experimental diffraction data for variously substituted Ti−CGC species.[2g,15] Thus, for example, lengthening of the Ti−N bond is observed on passing from $(CH_3)_2Si[(CH_3)_4C_5)](i\text{-PrN})Ti(CH_3)_2$ to $(CH_3)_2Si[(CH_3)_4C_5)](t\text{-BuN})Ti(CH_3)_2$ (1.895(4) to 1.957(7) Å, respectively).[2g]

Computed Molecular Structures of the $R_2Si(\eta^5\text{-}R'_4C_5)(R''N)TiR'''^+$ Naked Cations. The naked $R_2Si(R'_4C_5)(R''N)TiCH_3^+$ cations (**3a**−**d**) adopt a pseudo-trigonal-planar arrangement at Ti (Figure 2; Table 2). The molecules possess C_s symmetry, although the Ti−CH_3 bond vector can be readily displaced from the molecular (Cp centroid-Ti−N) plane; for example, a 50° bending incurrs less than 4 kcal/mol destabilization. The HF-derived bond angles and lengths involving the methyl group in the >Ti−CH_3^+ cation (∠Ti−C(1)−H(1), ∠Ti−C(1)−H(2), ∠Ti−C(1)−H(3), and C(1)−H(1), C(1)−H(2), and C(1)−H(3) in Figure 2) evidence deviations from local C_{3v} symmetry, which suggests significant α-agostic interactions[3,4] involving two σ(C−H) methyl−metal bonds [C(1)−H(1) and C(1)−H(2)]. These observations agree well with the electron-deficient character of the naked cations and, in turn, with the electronic structure alterations accompanying the cation-generating methide abstraction process. The two σ_{Ti-C} bonds of the neutral precursor molecules **1** involve the d_{xz} (out-of-the-phase combination) and d_{x2-y2} (in-the-phase combination) metal orbitals. Upon methide abstraction (eqs 2 and 3) by the Lewis acid cocatalyst, a vacant orbital site is generated at the metal, and the remaining CH_3 group can interact with either the d_{x2-y2} metal orbital, which leads to a C_s symmetric trigonal planar structure, or with the d_{xz} metal orbital, which leads to a trigonal pyramidal structure. These orbital relationships provide a convincing explanation for the substantial flexibility (with respect to out-of-plane bending) of the Ti−CH_3 bond vector in the naked cations because a suitable vacant orbital remains on the metal in both geometries and, therefore, secondary agostic interactions involving σ_{C-H} and/or σ_{C-C} alkyl bonds can be effective in flattening the potential energy surface. In the present cases (**3a**−**d**), the direct σ_{Ti-C} bond involves the Ti d_{x2-y2} orbital, while the d_{xz} orbital acts as an electron acceptor site for α-agostic interactions with one of the two degenerate, localized (C_{3v}) C−H (methyl) orbitals (**B**). Therefore, the α-agostic interaction drives the formation of the observed planar equilibrium geometry.

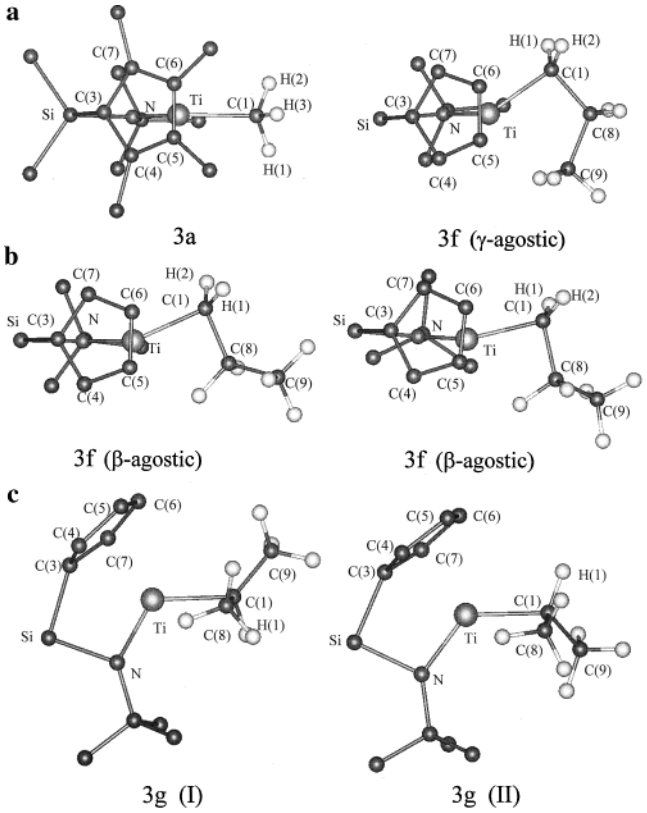

Figure 2. Molecular structures of selected naked cation systems: **3a**, $(CH_3)_2Si[(CH_3)_4C_5](t\text{-BuN})TiCH_3^+$; **3f**, $H_2Si(C_5H_4)(t\text{-BuN})TiCH_2CH_2\text{-}CH_3^+$ in the conformation having γ-agostic and β-agostic (two) interaction; and **3g,** $H_2Si(C_5H_4)(t\text{-BuN})TiCH(CH_3)_2^+$ in two possible conformations. Hydrogen atoms on the $R_2Si(C_5R'_4)(R''N)$ ligand have been omitted for clarity.

B

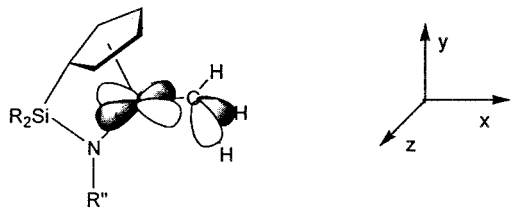

The foregoing observations can be contrasted with the computed equilibrium geometry of the hydride derivative, $H_2Si(C_5H_4)(t\text{-BuN})TiH^+$, in which the Ti−H bond is found to be displaced ∼41° out of the Cp centroid-Ti−N plane, while the C_s planar structure is 1.0 kcal/mol higher in energy at the MP2/HF level. In the hydrido cation, the lack of a possible agostic interaction, combined with a more directed (relative to a planar configuration) bonding interaction with the vacant d_{xz} metal orbital, favors the bent conformation, which is similar to the situation found in $(C_5H_5)_2TiH^+$.[16]

Upon homologation of the alkyl chain, specifically in the *n*-propyl cation $H_2Si(C_5H_4)(t\text{-BuN})TiCH_2CH_2CH_3^+$, three $TiCH_2CH_2CH_3$ conformations are found to be the most stable (they are nearly degenerate, with $\Delta E \leq 1$ kcal/mol). These structures are related by simple ∼120° rotation about the C(1)−C(8) bond. In all cases, the Ti−C(1) bonds lie out of the Cp centroid-Ti−N plane, and one of three σ bonds, C(8)−C(9), C(8)−H, or C(8)−H, is directed toward the vacant Ti coordination site. These conformers (Figure 2) can be described as γ or β agostic metal-propyl structures because they exhibit significant covalent interactions[3,4] involving the C_γ or C_β atoms. The more interesting structural features are (i) the Ti···C(9)H_3 distance (2.515 Å) in the γ-agostic conformation (**3f**) or the Ti···H−C(8)H distance (∼2.19 Å) in the two β-agostic structures (**3f**) are only slightly longer than the direct Ti−C (2.033 Å) or Ti−H (1.636 Å) σ bonds in the $TiCH_3^+$ (**3c**) and TiH^+ (**3e**) cations, respectively; (ii) in the γ-agostic structure, two C−H bonds of the C(9)H_3 methyl and the C(8)−C(9) bond distance are slightly elongated versus the unaffected C−H and C−C bonds, while only one C(8)−H σ bond is slightly longer (∼0.05 Å) than the other C−H bonds in the β-agostic structure; (iii) the Ti−C(1)−C(8) bond angles in the three *n*-propyl conformers (91.6°, 88.4°, and 90.2°, respectively) differ markedly from that expected for typical sp^3 hybridization at the C(1) atom. Note that β- and γ-agostic interactions are more efficient than α-agostic interactions in stabilizing transition metal cations because they allow better overlap between vacant metal orbital sites and the filled $\sigma_{C-H}/\sigma_{C-C}$ bonding orbitals of the alkyl chain. These findings are in agreement with previous theoretical studies of related naked cations.[3,4]

In the case of isopropylmetal cation $H_2Si(C_5H_4)(t\text{-BuN})TiCH(CH_3)_2^+$, four stable conformations are found. In all cases, these structures exhibit strong β-agostic interactions between the Ti center and the C(8) or C(9) methyl groups, with the Ti−C(1) vector displaced only a few degrees out of the Cp centroid-Ti−N plane. The four conformations can be interconverted by simple rotation of the isopropyl group about the Ti−C(1) bond. Note that the two structures in which C(8) is involved in a β-agostic interaction (**3g**, Figure 2) are equivalent by symmetry to the two structures in which C(9) is involved in the β-agostic interaction (not shown in Figure 2). The two conformations shown in Figure 2 are close in energy [structure **3g** (**I**) is 1.5 kcal/mol more stable than **3g** (**II**)], and conformation **3g** (**I**) minimizes the nonbonded repulsion between the C(9)H_3 group and the *t*-Bu group, while **3g** (**II**) minimizes steric repulsion with the Cp group. The Ti···H−C(8)H_2 and the C(8)−H distances, as well as the Ti−C(1)−C(8) bond angle, are similar to those found in **3f** (vide infra; Table 2).

Within the CGC series having constant cyclopentadienyl and alkylamido ancillary ligands, the more electron-donating R‴ substituents diminish the metal electrophilicity, and the total calculated Ti charges, +1.42, +1.40, +1.31, and +1.25 eu, respectively, fall in the order:

3e (hydride) > **3c** (methyl) > **3f** (*n*-propyl) > **3g** (isopropyl)

The nature of the R′ and R″ substituents on the ancillary ligands coordinated to the >Ti−CH_3 moiety similarly lowers the metal charge in the order:

3d > **3c** > **3a** ≈ **3b**,

with total computed Ti charges of +1.44, +1.40, +1.35, and +1.34 eu., respectively, upon increasing the R/R′/R″ electron donor character. From these results, it is apparent that modulation of the Ti electrophilicity by the metal alkyl group and ancillary ligand substituents is likely to be a major factor as far as the energetics of ion pair formation (eq 2) and heterolysis (eq 3) are concerned. These issues are explored further in the following sections in which catalyst−cocatalyst ion pairs are examined.

Molecular Structures of $R_2Si(\eta^5\text{-}R'_4C_5)(R''N)TiR'''\cdot CH_3B(C_6F_5)_3$ Catalyst-Cocatalyst Contact Ion Pairs. All of the Ti centers in complexes **2a**−**g**, activated with $B(C_6F_5)_3$, possess pseudotetrahedral coordination geometries with asymmetrically bonded alkyl ligands (Figure 3, Table 3). Considering the complexity of the calculation, there is good agreement between computed and experimental[15] ion pair metrical parameters (additional comments are made below). The CH_3−Ti−CH_3 angle remains nearly constant (∼100°) upon $B(C_6F_5)_3$ activation, while the length of the activated Ti−CH_3 bond undergoes considerable elongation (ΔTi−C(2) = 0.30−0.45 Å) versus the corresponding neutral precursor, and the remaining Ti−CH_3 bond length is significantly contracted (ΔTi−C(1) ∼ −0.03 Å). Consideration of the aforementioned bond lengths and computed Ti−C(2) bond orders of ∼ 0.33 in complexes **2a**−**g** would suggest that the activated/transferred CH_3 group remains partially bonded to the Ti center. The methyl hydrogen atoms, however, undergo a conformational inversion (Figure 3), thus bridging the metal center with an approximately linear Ti−H_3C−B vector (∠Ti−C−B = 170°−175°). The $R_2Si(R'_4C_5)(R''N)TiR'''^+\cdots H_3CB(C_6F_5)_3^-$ bonding interaction involves primarily the methido C_{2p} lone-pair with a bond order of ∼ 0.33. A contour plot of the 173a MO (Figure 4) of $H_2Si(C_5H_4)(t\text{-BuN})Ti(CH_3)\cdot H_3CB(C_6F_5)_3$, formally representing this interaction in a localized bonding model, reveals appreciable $C(2)_{2p}$ density directed toward both the B and Ti atoms. However, Mulliken MO population data reveal only minor (∼4%) metal character, thus suggesting a largely ionic bond. There is also indication of some bridging μ^3−Ti···H_3C−B interaction, principally contained in the 145a, 147a, and especially the 173a MO, with a minor Ti−$H_{average}$ bond index of ∼0.05.

The present unusual Ti···C−B bonding characteristics allow substantial energetic/geometric flexibility in the positioning of the C(2)H_3 group along the Ti−C(2)−B vector. The computed metrical data in Table 3 also evidence a remarkable dependence of the Ti···H_3C(2) bond distance upon the nature of the R′, and R‴ ligand substituents. Thus, comparable Ti···C(2)B distances (∼2.41 Å) are found for complexes **2b**−**d**, **f**, and **g**, while either contracted or elongated contacts are found for hydrido complex **2e** (2.348 Å) and Me_4C_5 complex **2a** (2.532 Å), respectively. The Ti···H_3C(2)−B$(C_6F_5)_3$ bond distances can be, in principle, influenced both by (i) electronic effects (stabilization of the

(16) Lauher, J. W.; Hoffmann, R. *J. Am. Chem. Soc.* **1976**, *98*, 1729.

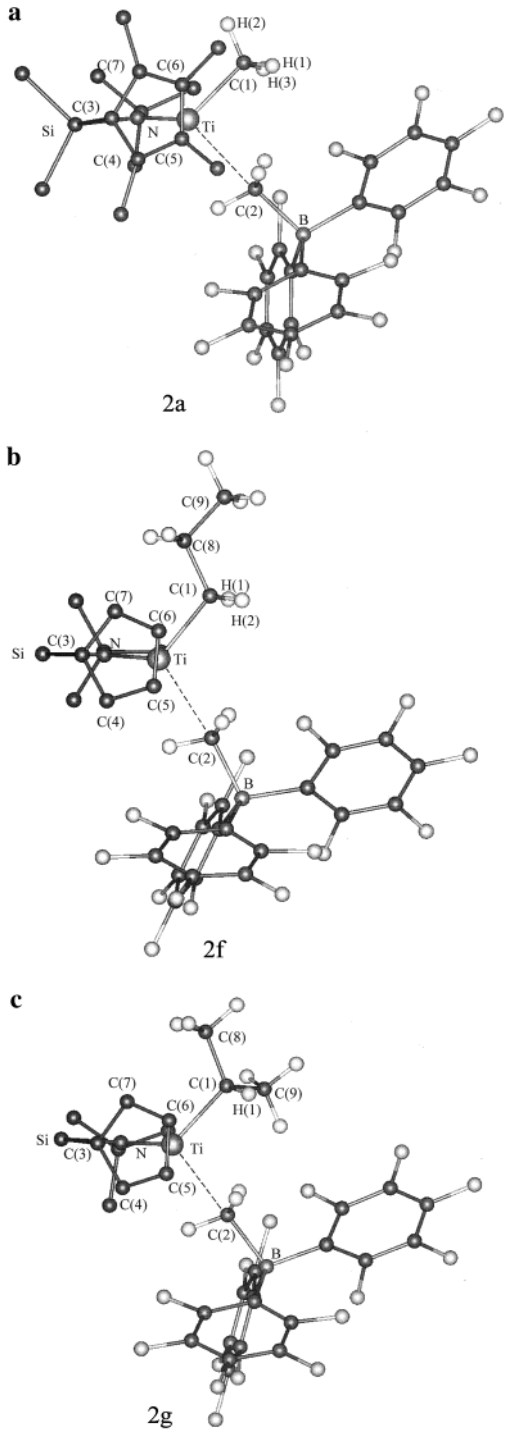

Figure 3. Molecular structures of selected contact ion pair adducts: **2a**, $(CH_3)_2Si[(CH_3)_4C_5](t\text{-BuN})Ti(CH_3)\cdot H_3CB(C_6F_5)_3$; **2f**, $H_2Si(C_5H_4)(t\text{-BuN})Ti(CH_2CH_2CH_3)\cdot H_3CB(C_6F_5)_3$; and **2g**, $H_2Si(C_5H_4)(t\text{-BuN})Ti(CH(CH_3)_2)\cdot H_3CB(C_6F_5)_3$. Hydrogen atoms on the $R_2Si(C_5R'_4)(R''N)$ ligand have been omitted for clarity.

electron-deficient cationic metal center) and/or by (ii) nonbonded repulsions between the ancillary ligand array surrounding the Ti center and the $CH_3B(C_6F_5)_3^-$ anion. In the present cases, the relative importance of steric vs electronic factors cannot be easily partitioned. Nevertheless, the observation that the total computed charges on the $H_3CB(C_6F_5)_3^-$ anion (−0.66 eu) and on the Ti center (1.29 eu) remain essentially constant throughout the present series suggests that electronic effects likely exert a constant influence on the equilibrium structures. Conversely, steric encumbrance in the space volume affected by the

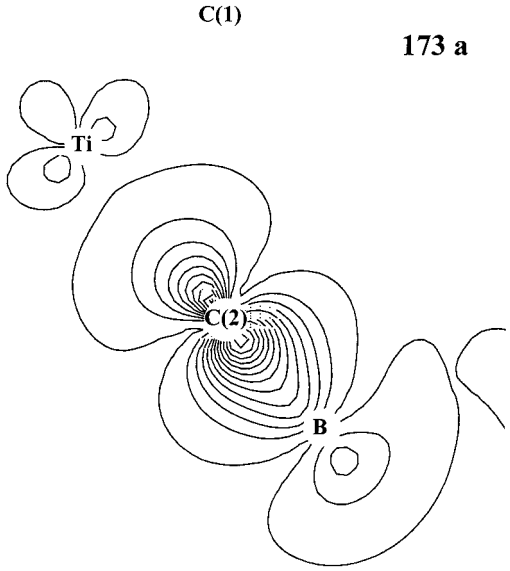

Figure 4. Electron density contour plot for the 173a MO in the Ti−C(2)−B plane of the $H_2Si(C_5H_4)(t\text{-BuN})Ti(CH_3)\cdot H_3CB(C_6F_5)_3$, **2c**, contact ion-pair adduct (atom C(1) lies 0.1 Å out of this plane). The contour step is 0.005 e/au^3.

contacting cocatalyst anion provides a convincing rationale for the shorter Ti···$H_3C(2)$ bond in complex **2e**, where the smaller hydrido ligand (versus CH_3) allows more room for a $H_3CB(C_6F_5)_3^-$ approach. Conversely, the significant steric crowding introduced by the permethylated Cp ring in complex **2a** induces a longer Ti···$H_3(C2)$ bond distance. Finally, the Ti−C(1) bond distance in the present systems contracts upon lowering the σ-donor character (and reducing the steric demands) of the metal-alkyl ligand, namely, **2g** (R‴ = isopropyl) > **2f** (R‴ = *n*-propyl) > **2c** ≈ **2d** (R‴ = methyl). Interestingly, Cp permethylation and H_2Si< → $(CH_3)_2Si$< bridge methylation induce modest elongation of the Ti−C(1) bond distance (**2a** > **2b** > **2c**), presumably reflecting increased electron donor character and increased steric congestion.

The computed metrical parameters for $(CH_3)_2Si[(CH_3)_4C_5](t\text{-BuN})Ti(CH_3)\cdot CH_3B(C_6F_5)_3$ (**2a)** in Table 3 are generally in favorable agreement with X-ray diffraction data for the ion pair.[15] Nevertheless, a slightly longer (0.168 Å) Ti−C(2) distance versus the experimental value [2.364(3) Å] is computed. Two factors appear to be responsible for this disparity: (i) the use of uncorrelated wave functions (a 0.06 Å shortening is observed for the $H_2Si(C_5H_4)(CH_3N)Ti(CH_3)\cdot CH_3BF_3$ model on passing from the HF to MP2 optimized structure)[9b] and (ii) crystal packing forces. In all of the present catalyst−cocatalyst adducts, the B atom assumes a pseudotetrahedral coordination environment, which represents a reorganization of the trigonal planar geometry found in $B(C_6F_5)_3$. The computed B−C(C_6F_5) bond lengths (1.664 Å average) and C(C_6F_5)−B−C(C_6F_5) bond angles (111.6° average) lie, however, between the values found in "free" $B(C_6F_5)_3$ (B−C = 1.577 Å; ∠C(C_6F_5)−B−C(C_6F_5) = 120°)[1a] and those in the "free" $CH_3B(C_6F_5)_3^-$ anion (B−C = 1.687 Å; C(C_6F_5)−B−C(C_6F_5) = 109.6°).[1a] These observations suggest somewhat reduced B−C(C_6F_5) π-bonding in the ion pairs due to significant $sp^2 \rightarrow sp^3$ rehybridization at the B atom.

It is of importance for understanding the actual catalytic systems to compare and contrast the electronic structures and geometries of the ion-paired, activated complexes **2** (Table 3) with those of the free cations **3** (Table 2). As noted above, pseudotrigonal arrangements around Ti are found in methyl

Table 3. Computed HF and Experimental Bond Lengths (Å) and Angles (deg) in $R_2Si(\eta^5\text{-}R'_4C_5)(R''N)TiR'''^+ \cdot H_3CB(C_6F_5)_3^-$ Catalyst-Cocatalyst Contact Ion Pairs (2)

	2a R = R′ = R‴ = CH_3 R″ = *t*-Bu	**2b** R = R‴ = CH_3 R′ = H R″ = *t*-Bu	**2c** R = R′ = H R″ = *t*-Bu R‴ = CH_3	**2d** R = R′ = H R″ = R‴ = CH_3	**2e** R = R′ = R‴ = H R″ = *t*-Bu	**2f** R = R′ = H R″ = *t*-Bu R‴ = nPr	**2g** R = R′ = H R″ = *t*-Bu R‴ = *i*-Pr
			Bond length[a,b]				
Ti−C(1)	2.064 (2.087(4))	2.055	2.051	2.049	(1.618)	2.050	2.103
Ti−C(2)	2.532 (2.364(3))	2.397	2.435	2.415	2.348	2.418	2.392
Ti−Cp centroid	2.098 (2.029)	2.119	2.125	2.113	2.094	2.129	2.151
Ti−N	1.896 (1.904(3))	1.875	1.872	1.859	1.862	1.878	1.884
N−Si	1.839 (1.757(3))	1.843	1.830	1.814	1.828	1.828	1.828
Si−C(3)	1.910 (1.858(4))	1.895	1.884	1.891	1.891	1.885	1.880
C(2)−B	1.713 (1.675(5))	1.707	1.710	1.710	1.711	1.706	1.707
$B-C(C_6F_5)_{av}$	1.669 (1.651(5))	1.662	1.664	1.666	1.660	1.663	1.664
C(1)−H(1)	1.085 (1.09)	1.084	1.085	1.083		1.092	1.092
C(1)−H(2)	1.084 (1.09)	1.086	1.084	1.086		1.092	(1.538)[c]
C(1)−H(3)	1.086 (1.09)	1.085	1.086	1.090		(1.535)[d]	(1.545)[d]
			Bond angle[a,b]				
C(1)−Ti−C(2)	91.4 (100.8(1))	96.6	99.4	101.7	102.0	97.6	99.3
Θ[e]	49.8 (42.3)	51.0	53.6	56.0	64.2	62.0	48.7
N−Ti−Cp centroid	110.1 (110.2)	109.8	109.3	107.9	110.2	109.5	109.0
Ti−N−Si	103.4 (103.8(1))	103.8	103.9	106.0	103.5	103.4	103.5
N−Si−C(3)	89.6 (91.1(1))	90.0	90.9	89.8	90.4	89.0	91.6
Ti−C(2)−B	174.6 (170.2(2))	170.5	175.2	175.6	172.1	170.0	172.0
Ti−C(1)−H(1)	113.3 (109.5)	112.7	112.0	112.6		101.4	98.9
Ti−C(1)−H(2)	108.4 (109.4)	108.5	108.4	108.0		105.2	(115.9)[f]
Ti−C(1)−H(3)	109.4 (109.5)	109.5	110.9	110.1		(122.1)[g]	(116.5)[g]
$C(2)-B-C(C_6F_5)_{av}$	107.6 (108.6(3))	106.9	107.6	107.9	107.1	107.3	107.0

[a] Experimental data from ref 15 in parentheses. [b] Atom labeling defined in Figure 3. [c] C(1)−C(9) bond length. [d] C(1)−C(8) bond length. [e] Angle between the Cp centroid-Ti−N plane and the Ti−C(1) vector. [f] Ti−C(1)−C(9) bond angle. [g] Ti−C(1)−C(8) bond angle.

cations **3a**−**d** with the Ti−CH_3 vector lying in the Cp centroid-Ti−N plane. Slightly bent pyramidal structures are apparent in propyl cations **3f**, **g**. In the catalyst−cocatalyst adducts, the Ti−C(1)H_3 vector is invariably displaced ∼50° out of the Cp centroid-Ti−N plane, while the Ti−Cp centroid, Ti−C(1), and Ti−N bond lengths become longer relative to those of the parent naked cations. Other important structural modifications are associated with the alkyl chain that is bonded to the C(1) atom upon methide abstraction (eq 3). Thus, the internal hydrocarbyl Ti−C(1)−H angles and C(1)−H distances in adducts **2** are close to those expected for classical, neutrally charged metal dialkyls in contrast to the highly distorted geometries of the electron-deficient parent cations (**3**). This observation is consistent with experimental evidence[6] for weaker (than in naked cations) or negligible agostic interactions in the ion pairs.

Significant rearrangements of the *n*-propyl- and isopropyl-metal moieties relative to the naked cations occur upon $H_3CB(C_6F_5)_3^-$ coordination. Thus, those components of the alkyl groups formerly directed toward the electrophilic vacant metal coordination site are displaced far from the cationic metal center in the ion pair complexes. In the case of isopropyl derivative **2g**, only one stable conformation is found, while various conformers lie close in energy for *n*-propyl-metal complex **2f** (Figure 3 and Table 3 report only the most stable structures). The computed metrical parameters indicate some deviations from those expected for sp^3 hybridization at C(1). In fact, the computed Ti−C(1)−H(1) and Ti−C(1)−H(2) bond angles in the *n*-propyl group and Ti−C(1)−H(1) bond angles in the isopropyl group (**2f**, **g**; Table 3) are somewhat smaller than 109.5°. These deviations are likely due to the differing steric requirements of the neighboring CH_3 and H groups.

It is well-known that in metallocenium ion pairs involving $B(C_6F_5)_4^-$ and related counteranions, coordination to the metal centers occurs via long metal···fluorine(aryl) contacts.[1a,6b,i,k] This information motivated an in-depth search in the present study for similar types of Ti···F(aryl) coordination in $H_2Si(C_5H_4)$(*t*-BuN)Ti(CH_3)·$H_3CB(C_6F_5)_3$. Several structures with Ti···F coordination were found to be energetically accessible. However, they invariably lie somewhat higher in energy with respect to μ-CH_3 coordination. For example, the structure in Figure 5 (calculated Ti−F bond distance = 2.084 Å) is found to lie ∼5 kcal/mol above the ground state μ-CH_3 geometry at the HF level, and the large variety of related structures lying close in energy is an indication of the stereochemical flexibility of the $Ti^+\cdots H_3CB(C_6F_5)_3^-$ linkage. Nevertheless, the preferred coordination mode to Ti (versus fluorine) is invariably via CH_3, which is a consequence of the considerable electron density accumulation on this group. These results, and in particular the

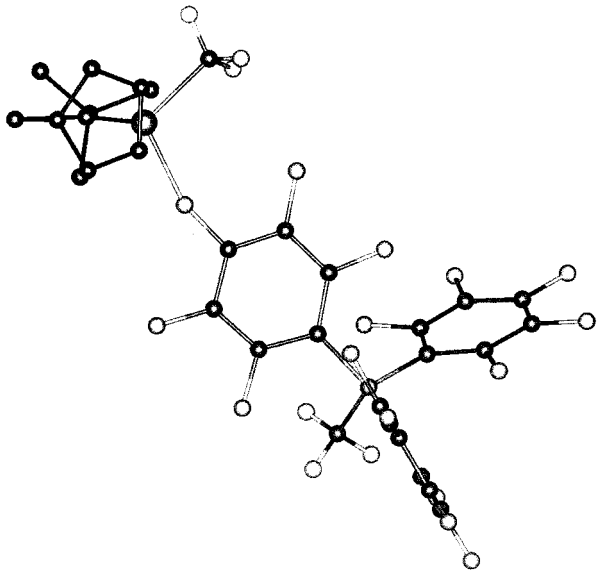

Figure 5. Molecular structure of $H_2Si(C_5H_4)$(*t*-BuN)Ti(CH_3)·$H_3CB(C_6F_5)_3$, **2c**, in which a fluorine atom, rather than the CH_3 group of the $H_3CB(C_6F_5)_3^-$ anion, coordinates to the metal center. Hydrogen atoms on the $H_2Si(C_5H_4)$(*t*-BuN) ligand have been omitted for clarity.

Table 4. Catalyst−Cocatalyst Ion Pair Formation Enthalpies for the Process, $R_2Si(R'_4C_5)(R''N)Ti(R''')(CH_3) + B(C_6F_5)_3 \rightarrow R_2Si(R'_4C_5)(R''N)Ti(R''')\cdot H_3CB(C_6F_5)_3 + \Delta H_{form}$[a]

contact ion pair		HF	MP2	MP2/BSSE gas phase	MP2/BSSE C_6H_6 ($\epsilon = 2.27$))	MP2/BSSE C_6H_5Cl ($\epsilon = 5.71$))	MP2/BSSE CH_2Cl_2 ($\epsilon = 9.08$)
$(CH_3)_2Si[(CH_3)_4C_5](t\text{-BuN})Ti(CH_3)\cdot H_3CB(C_6F_5)_3$	**2a**	−1	−38	−14	−16	−16	−16
$(CH_3)_2Si(C_5H_4)(t\text{-BuN})Ti(CH_3)\cdot H_3CB(C_6F_5)_3$	**2b**	−2	−39	−15	−17	−17	−17
$H_2Si(C_5H_4)(t\text{-BuN})Ti(CH_3)\cdot H_3CB(C_6F_5)_3$	**2c**	3	−31	−10	−13	−13	−13
$H_2Si(C_5H_4)(CH_3N)Ti(CH_3)\cdot H_3CB(C_6F_5)_3$*	**2d**	2	−32	−10	−13	−13	−14
		(−3)	(−31)	(−11)	(−14)	(−15)	(−16)
$H_2Si(C_5H_4)(t\text{-BuN})TiH\cdot H_3CB(C_6F_5)_3$	**2e**	2	−34	−11	−12	−13	−13
$H_2Si(C_5H_4)(t\text{-BuN})Ti(CH_2CH_2CH_3)\cdot H_3CB(C_6F_5)_3$	**2f**	−1	−36	−12	−14	−14	−14
$H_2Si(C_5H_4)(t\text{-BuN})Ti[CH(CH_3)_2]\cdot H_3CB(C_6F_5)_3$	**2g**	2	−33	−10	−12	−12	−12

[a] Data in kcal/mol. Values in parentheses refer to calculations including polarization function.

variety of energetically accessible fluorine metal-bonded geometries that were located, differ somewhat from those found in a recent DFT analysis of the $(C_5H_5)_2Ti(CH_3)\cdot(CH_3)B(C_6F_5)_3$ system.[5b] In this case, there is indication that the only energetically accessible structure involves μ-CH_3 coordination because all of the Ti···F(aryl)-bonded ion pairs lie substantially higher in energy (>15.4 kcal/mol). While the DFT computations consider a somewhat different ancillary ligand system than that presently analyzed, the results are surprising in view of the experimental evidence for ubiquitous flexibility of the cation−anion bonding in such systems.[6]

Energetic Aspects of Ion Pair Adduct Formation. At the HF level, the formation of catalyst−cocatalyst contact ion pairs with $B(C_6F_5)_3$ (eq 2) appears to be unfavorable on thermodynamic grounds (Table 4). However, at the MP2 level, all of the species are bound, due to the expected stabilizing contribution of correlation energies that are associated with bond formation. It is interesting to note that the MP2-derived ΔH_{form} values are consistently more negative (more exothermic) than experimental, but are reduced considerably by the inclusion of BSSE corrections (the BSSE effect is almost constant for all species, ∼23 kcal/mol). Calculations including polarization functions for $H_2Si(C_5H_4)(CH_3N)Ti(CH_3)\cdot H_3CB(C_6F_5)_3$ yield a minor increase in reaction exothermicity (1 kcal/mol) and a slight reduction of BSSE correction (2 kcal/mol; Table 4). Because of the similar geometrical arrangements and electronic structures of all species considered, we can safely assume that any improvement of calculations has a scaling effect on computed energies (see also the discussion of solvent molecule complexation below). The theoretical value (−14 kcal/mol in the gas phase) thus inferred for $(CH_3)_2Si[(CH_3)_4C_5](t\text{-BuN})Ti(CH_3)\cdot H_3CB(C_6F_5)_3$ formation (eq 2) lies close to the thermochemical titration result (−22.6(2) kcal/mol)[6e] that was obtained in toluene solution. The inclusion of nonspecific solvation effects slightly improves the calculated result (−16 kcal/mol), and better agreement with experiment is thereby obtained. This computed ΔH_{form} value improves the agreement between theory and experiment relative to that previously reported[9] for the simplified $H_2Si(C_5H_4)(t\text{-BuN})Ti(CH_3)\cdot H_3CB(C_6F_5)_3$ model (−13 kcal/mol). The use of very extended basis sets and more accurate wave function expansions would doubtless improve the quantitative comparison to some degree; however, this currently represents a major computational task for any catalytically realistic ion pair. Moreover, the results of the present study evidence generally good agreement with experiment and allow important trends to be characterized.

The present energetic data for ion-pair formation (Table 4) reveal moderate dependence of ΔH_{form} on the ancillary ligand substituents, the alkyl fragment bonded to the metal, and the reaction solvent. For all systems considered, the calculated gas phase ΔH_{form} data are spread over a relatively narrow range (−10 to −12 kcal/mol), except for complexes **2a** and **b** where the ΔH_{form} values are somewhat more exothermic (−14 to −15 kcal/mol). This trend parallels the experimental ΔH_{form} data for several zirconium metallocenes.[6a,e,f] Thus, measured ΔH_{form} values for $(C_5H_5)_2Zr(CH_3)\cdot H_3CB(C_6F_5)_3$, $[1,2\text{-}(CH_3)_2C_5H_3]_2Zr(CH_3)\cdot H_3CB(C_6F_5)_3$, and $[1,2\text{-}(CH_3)_2C_5H_3]_2ZrCH_2Si(CH_3)_3\cdot H_3CB(C_6F_5)_3$, similarly lie in the narrow −22 to −25 kcal/mol range, while considerably larger values are determined for more sterically encumbered/electron-rich $[(CH_3)_5C_5]_2Zr(CH_3)\cdot H_3CB(C_6F_5)_3$ and $[1,2\text{-}(CH_3)_2C_5H_3]_2ZrCH[Si(CH_3)_3]_2\cdot H_3CB(C_6F_5)_3$ (ΔH_{form}= −36.7(5) and −59.2(1.4) kcal/mol, respectively),[6a,b,e,f] where the substantial crowding in the neutral dialkyl precursors is presumably relaxed upon $B(C_6F_5)_3$ coordination/CH_3^- abstraction, and the cation is stabilized electronically as well (vide infra).

The ΔH_{form} calculations also reveal (Table 4) that the energetics of methide abstraction are slightly influenced by solvent, involving a few kcal/mol variation on passing either from the gas phase to solution or from lower to higher dielectric constant solvents. Unfortunately, no experimental data are available for solvation effects on the formation enthalpy of $(CH_3)_2Si(C_5H_4)(t\text{-BuN})Ti(CH_3)\cdot H_3CB(C_6F_5)_3$. Nevertheless, the present trend agrees well with experimental ΔH_{form} data measured for $[1,2\text{-}(CH_3)_2C_5H_3]_2MCH_3\cdot H_3CB(C_6F_5)_3$ complexes (M = Zr, Hf) in toluene and chlorobenzene. In both cases, small stabilizations (2−8 kcal/mol) are observed in the more polar solvent.[6d]

Recent DFT studies of model ion pair **2c** yielded ΔH_{form} = −18.0 kcal/mol,[5b] which is in close agreement with the experimental value for **2a**. The present ab initio calculations yield −14 kcal/mol (including effects of polarization functions). To understand this moderate disparity, note that the major parameters affecting ΔH_{form} values should be the variation of electron correlation upon bond formation. Any calculation including the exact evaluation of electron correlation would require very large basis sets and the inclusion of triple and quadruple excitations in the wave function expansions. Although this certainly represents a current limit to ab initio methodologies for large systems, it is also known that DFT approaches can overestimate electron correlation,[10] with the consequent fortuitous balance of basis set truncation. The present ab initio results reveal a small but significant increase in ΔH_{form} with solvent polarity, which is in agreement with chemical intuition. Indeed, methide abstraction induces a large reorganization of the electron density from the precatalyst toward the $B(C_6F_5)_3$ group, thus creating a significant charge separation. This induces a large change in dipole moment [$B(C_6F_5)_3$ μ = 0 D; precatalyst $\mu \approx$ 1 D; contact ion pair $\mu \approx$ 16 D] which, even at a qualitative

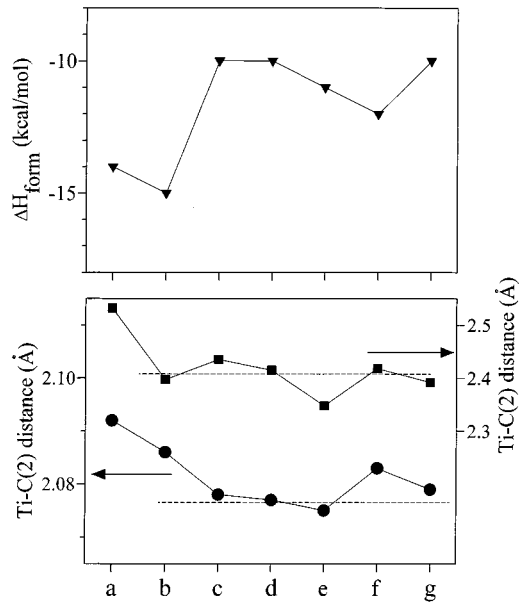

Figure 6. Methide abstraction enthalpies (top) for the complexes presently considered. Ti−C(2) bond distance (bottom) in contact ion pair (■ scale on the right) and precatalyst (● scale on the left). Dashed lines refer to average values.

level of analysis, should result in product stabilization by higher dielectric solvents.

The measured energetics of methide abstraction reflect, for fixed Lewis acid cocatalyst and minimal solvation effects, an interplay of the relative stabilities of the precatalyst and the contact ion pair. These, in turn, reflect a balance between the Ti−C(2)H_3 homolytic bond dissociation enthalpy plus the $R_2Si(R_4'C_5)(R''N)TiR'''$ ionization potential, versus the $\cdot CH_3$ electron affinity plus the borane CH_3^- affinity plus the ion pairing enthalpy.[6a,b,e,f] It was found that the bond length modulation along the Ti···C(2)−B$(C_6F_5)_3$ vector as a function of interacting catalyst-cocatalyst system parallels many of the observed ΔH_{form} trends, because such distances are doubtless indices of the bonding forces operative. In all of the present precatalyst molecules, the Ti−CH_3 bond was found to be largely covalent in nature, with a 30−40% metal contribution. Even small bond elongation/weakening effects require large energies and result in commensurately large destabilization effects. Upon interacting with B$(C_6F_5)_3$, the same Ti−C(2) bond evolves into an essentially ionic bond (∼4% metal contribution) describable by a softer potential well, as a strong $H_3C-B(C_6F_5)_3^-$ covalent bond is formed (Figure 4). The computed and experimental bond distance data in Table 3 argue that the anion subunit remains relatively insensitive to the nature of the precatalyst. An obvious consequence is that ion pair stabilization, hence exothermic ΔH_{form} values, must involve endothermic processes (Ti−CH_3 homolysis; $R_2Si(R_4'C_5)(R''N)TiR'''$ ionization) favorably balanced by the stabilizing, exothermic counterparts noted above. Note in addition that the energy required for Ti−CH_3 elongation becomes of minor structural relevance once the ion pair adduct is formed due to the ionic nature of the resulting cation−anion interaction. For instance, and as will be discussed in the following section, 7 kcal/mol is required for a 0.6 Å elongation of the Ti···C(2) bond in ion pair adduct **2c,** while the same enthalpy input achieves only a 0.25 Å Ti−C bond lengthening in the neutral parent precatalyst **1c**.

The Ti···C(2) distances in ion pairs **2b**−**d**, **f**, and **g** have an average calculated value of 2.41 Å (range = 2.392−2.435 Å; Figure 6, Table 3). This same parameter is slightly larger in **2a** (2.532 Å; R′ = CH_3) and smaller in **2e** (2.348 Å; R‴ = H). The precursor Ti−C(1) distances are nearly constant (∼2.077 Å) in **1c**−**e,** and **g** while a somewhat greater dispersion is observed in **1a** (R′ = CH_3, R‴ = CH_3), **1b** (R′ = H, R‴ = CH_3), and **1f** (R‴ = *n*-propyl; Figure 6, Table 1). As noted above, the trend in computed gas-phase ΔH_{form} values (Figure 6, Table 4) exhibits similar exothermicities (−10 kcal/mol) for complexes **2c**−**e** and **g**, while slightly greater exothermicities are calculated for more electron-rich **2f** (−12 kcal/mol), **a**, and **b** (−15 kcal/mol). Interestingly, it appears that the greater stabilization of ion pairs **2a**, **b**, and **f** roughly parallels the greater Ti−CH_3 distances in the corresponding precatalysts. These arguments provide a rationale for the substituent effects on ΔH_{form} and possibly for some trends in catalytic properties. Upon replacing the H ligand in the Ti hydride with more sterically encumbered alkyl ligands [R‴ = CH_3, $CH_2CH_2CH_3$, and $CH(CH_3)_2$], only modest variations in ΔH_{form} are observed, possibly because any enhanced donor capacity and weaker Ti−C(2) bonding of the alkyl ligands is counterbalanced by the greater, sterically induced, destabilizing Ti···C(2) elongation in the product. Methylation of the Si bridge and Cp ligand introduce both additional electron donor capacity as well as steric encumberance. Similarly, the greater catalytic activity of **1a** relative to **1b** may reflect, among other factors, the longer Ti−C(2)H_3 distance/weaker bonding in **2a** and greater, sterically enforced cation−anion separation (vide infra) which, in turn, may render the metal center more reactive with respect to olefin activation/enchainment.

Energetics of Heterolytic Ion Pair Separation. Gas-phase ion pair separation reactions (eq 3) are invariably computed to be strongly endothermic at both the HF and MP2 levels (Table 5). As in the case of methide abstraction, the BSSE correction significantly reduces the MP2 values. Calculations including polarization functions for $H_2Si(C_5H_4)(CH_3N)Ti(CH_3)\cdot H_3CB(C_6F_5)_3$ show an increase in heterolytic ion-pair separation enthalpy (by ∼8 kcal/mol), while the BSSE is slightly reduced

Table 5. Heterolytic Ion Pair Separation Enthapies for the Process, $R_2Si(R'_4C_5)(R''N)Ti(R''')\cdot H_3CB(C_6F_5)_3 \rightarrow R_2Si(R'_4C_5)(R''N)Ti(R''')^+ + CH_3B(C_6F_5)_3^- + \Delta H_{ips}$[a]

				MP2/BSSE			
contact ion pair		HF	MP2	gas phase	C_6H_6 (ϵ = 2.27))	C_6H_5Cl (ϵ = 5.71)	CH_2Cl_2 (ϵ = 9.08)
$(CH_3)_2Si[(CH_3)_4C_5](t\text{-BuN})Ti(CH_3)\cdot H_3CB(C_6F_5)_3$	**2a**	66	93	75	40	22	17
$(CH_3)_2Si(C_5H_4)(t\text{-BuN})Ti(CH_3)\cdot H_3CB(C_6F_5)_3$	**2b**	76	100	79	44	26	20
$H_2Si(C_5H_4)(t\text{-BuN})Ti(CH_3)\cdot H_3CB(C_6F_5)_3$	**2c**	76	96	78	43	23	19
$H_2Si(C_5H_4)(CH_3N)Ti(CH_3)\cdot H_3CB(C_6F_5)_3$*	**2d**	81	100	83	47	28	24
		(84)	(107)	(91)	(55)	(37)	(33)
$H_2Si(C_5H_4)(t\text{-BuN})TiH\cdot H_3CB(C_6F_5)_3$	**2e**	85	107	89	48	22	16
$H_2Si(C_5H_4)(t\text{-BuN})Ti(CH_2CH_2CH_3)\cdot H_3CB(C_6F_5)_3$	**2f**	73	92	74	40	23	20
$H_2Si(C_5H_4)(t\text{-BuN})Ti[CH(CH_3)_2]\cdot H_3CB(C_6F_5)_3$	**2g**	68	86	68	34	17	16

[a] Data in kcal/mol. Values in parentheses refer to calculations including polarization function.

Table 6. Solvent Stabilization Energies of Precatalyst, Cationic Catalysts, Catalyst-Cocatalyst, $B(C_6F_5)_3$, and $CH_3B(C_6F_5)_3^-$ [a]

contact ion pair		precatalyst			cation			ion pair		
		C_6H_6	C_6H_5Cl	CH_2Cl_2	C_6H_6	C_6H_5Cl	CH_2Cl_2	C_6H_6	C_6H_5Cl	CH_2Cl_2
$(CH_3)_2Si(C_5(CH_3)_4)(t\text{-BuN})Ti(CH_3)\cdot H_3CB(C_6F_5)_3$	**2a**	−1	−2	−2	−27	−41	−45	−9	−15	−16
$(CH_3)_2Si(C_5H_4)(t\text{-BuN})Ti(CH_3)\cdot H_3CB(C_6F_5)_3$	**2b**	−1	−2	−2	−27	−41	−46	−9	−15	−16
$H_2Si(C_5H_4)(t\text{-BuN})Ti(CH_3)\cdot H_3CB(C_6F_5)_3$	**2c**	−1	−2	−2	−28	−44	−47	−10	−16	−17
$H_2Si(C_5H_4)(CH_3N)Ti(CH_3)\cdot H_3CB(C_6F_5)_3$	**2d**	−1	−2	−2	−29	−44	−48	−10	−16	−18
		(−1)	(−2)	(−2)	(−28	(−43)	(−47)	(−9)	(−15)	(−17)
$H_2Si(C_5H_4)(t\text{-BuN})TiH\cdot H_3CB(C_6F_5)_3$	**2e**	−2	−2	−3	−33	−55	−61	−9	−15	−17
$H_2Si(C_5H_4)(t\text{-BuN})Ti(CH_2CH_2CH_3)\cdot H_3CB(C_6F_5)_3$	**2f**	−1	−2	−2	−26	−39	−41	−9	−15	−16
$H_2Si(C_5H_4)(t\text{-BuN})Ti[CH(CH_3)_2]\cdot H_3CB(C_6F_5)_3$	**2g**	−1	−2	−2	−26	39	−40	−9	−15	−16

species	C_6H_6	C_6H_5Cl	CH_2Cl_2
$B(C_6F_5)_3$	−6	−11	−12
	(−5)	(−9)	(−10)
$(CH_3)B(C_6F_5)_3^-$	−17	−27	−29
	(−17)	(−26)	(−28)

[a] Data in kcal/mol. Values in parentheses refer to calculations including polarization function.

(by ∼1 kcal/mol). Table 6 reports nonspecific solvation energies that are associated with all of the species involved in eqs 2 and 3. Major stabilizing solvation effects are, not surprisingly, associated with charged species and reduce the ΔH_{ips} values significantly, the specifics depending on the solvent polarity. Thus, consistently larger enthalpy differences [ΔH_{ips}(gas phase) − ΔH_{ips}(solution) ≈ 35, ≈ 53, and ≈ 57 kcal/mol] are observed on passing from benzene (ϵ = 2.274) to chlorobenzene (ϵ = 5.71) to dichloromethane (ϵ = 9.08), respectively. These data agree with DFT results on (1,2 dimethyl-$C_5H_3)_2Zr(CH_3)_2$ plus various Lewis acids as a function of solvent polarity.[5a,b] In this case, large variations in ΔH_{ips} of ∼40, ∼60, and ∼63 kcal/mol are also observed for toluene (ϵ = 2.379), chlorobenzene (ϵ = 5.71) and dichlorobenzene (ϵ = 9.93), respectively. Even more interesting, the present ab initio results also agree with experimental dynamic NMR studies of ion-pair symmetrization rates in $[1,2\text{-}(CH_3)_2C_5H_3]_2ZrCH_3\cdot H_3CB(C_6F_5)_3$ (eq 5),[6a,b,e,f]

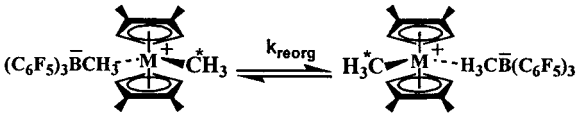

(5)

which indicate a very large enhancement (∼2000×) in rate on passing from toluene to chlorobenzene. More pronounced naked cation solvent stabilization is observed for the sterically less encumbered hydride derivative **2e** in the aforementioned solvents (41, 67, and 73 kcal/mol, respectively).

Ligand substituents also affect computed ΔH_{ips} values, and in particular, a sizable dependence on ancillary ligand substitution, as well as on the metal-bonded alkyl moiety, is observed (Table 5). The most endothermic enthalpy of ion pair separation is calculated for Ti hydride **2e**, while the lowest values (least endothermic) are found for fully ring-substituted species **2a** and for isopropyl derivative **2g**. The observed trend clearly reflects the electronic capacities of the various ligand arrays to stabilize the naked cations along with greater steric repulsion of the counteranion that was induced by the bulkier ligands. The two classes of ion pair systems that are presently considered (constant ancillary ligand, constant metal-alkyl group) allow convincing quantification of the role of agostic interactions and ancillary ligand substitution on ΔH_{ips}. Thus, complexes **2e**, **c**, **f**, and **g** with varying metal-alkyl group R‴, evidence progressive reduction of ΔH_{ips} (less endothermic) on passing from H to CH_3, $CH_2CH_2CH_3$, and $CH(CH_3)_2$ (Table 5). These data are in accord with the greater (versus H) electron donor capacity of CH_3 (more efficient stabilization of the cation) as well as with α-agostic interactions involving the CH_3 group. Even more important, ΔH_{ips} values decrease upon further homologation of the alkyl chain because such moieties are more electron-releasing and participate in strong β-agostic (or γ-agostic for *n*-propyl) interactions (vide supra). As noted above, β- and γ-agostic interactions are more stabilizing than α-agostic interactions because more effective overlap between C_β-C_γ and C_β-H bonds and suitable, empty metal orbitals is possible.[3,4] These results are also relevant to catalytic chain propagation because in some single-site systems, polymerization rates can be correlated with the "looseness" of the ion pairing.[1a,6d,e]

A noticeable effect on computed ΔH_{ips} values is also observed on passing from a primary *n*-propyl to a secondary isopropyl Ti cation (Table 5). This particular ordering doubtless reflects the greater σ-donor capacity of the secondary alkyl group along with steric effects, because comparable agostic interactions are found in both species (vide supra). Note also that the presently computed ΔH_{ips} values as a function of alkyl chain length approximately parallel the R-dependent $\Delta H^{\ddagger}_{reorg}$ trends recently obtained by dynamic NMR spectroscopy for $[1,2\text{-}(CH_3)_2C_5H_3]_2$-$Zr(R)\cdot H_3CB(C_6F_5)_3$ complexes (R = CH_3, $CH_2C(CH_3)_3$, CH_2-

(6)

R	$\Delta H^{\ddagger}_{reorg}$ (kcal/mol)
CH_3	22(1)
$CH_2C(CH_3)_3$	18(1)
$CH_2Si(CH_3)_3$	17(1)
$CH[Si(CH_3)_3]_2$	9(2)

$Si(CH_3)_3$, $CH[Si(CH_3)_3]_2$; eq 6).[6a] In fact, the incremental decrease of computed ΔH_{ips} with increasing alkyl chain length [H > CH_3 > $CH_2CH_2CH_3$ > $CH(CH_3)_2$] approximately parallels the diminution of the $\Delta H^{\ddagger}_{reorg}$ values [CH_3 > $CH_2Si(CH_3)_3$ ∼ $CH_2C(CH_3)_3$ > $CH[Si(CH_3)_3]_2$] that was observed experimentally.[6a] In addition, the data trends in Table 5 suggest that agostic interactions likely play a role in ion pair separation/reorganization energetics because they significantly stabilize the cationic species. The computed ΔH_{ips} values are also affected by ancillary ligand substitution (for constant alkyl chain; complexes **2a**−**d**). Thus, ΔH_{ips} is decreased both by replacing

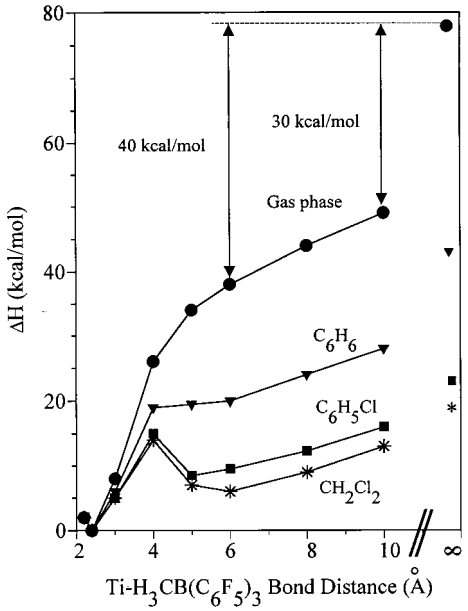

Figure 7. Enthalpic profile for heterolytic $H_2Si(C_5H_4)(t\text{-BuN})Ti(CH_3)^+\cdots H_3CB(C_6F_5)_3^-$ cleavage that was calculated in the gas phase (MP2/BSSE) and in benzene (C_6H_6), chlorobenzene (C_6H_5Cl), and dichloromethane (CH_2Cl_2) solutions. Values on the right refer to the completely separated $H_2Si(C_5H_4)(t\text{-BuN})TiCH_3^+$ and $H_3CB(C_6F_5)_3^-$ ions.

N-CH_3 with N-*t*-Bu or by substituting H on the bridging $>SiH_2$ unit and on the Cp ring with CH_3 groups. This trend again emphasizes the influence of electronic and steric factors on the endothermicity of heterolytic ion-pair separation because introduction of substituents with greater electron donor character or increased nonbonded repulsions invariably weakens the ion pairing by stabilizing the cationic species. It is likely that ion pairing looseness in some systems is kinetically significant in regard to olefin activation/enchainment and other sterically demanding catalytic processes.[1a,6]

These results provide evidence that ΔH_{ips} variations depend principally on electronic stabilization of the naked cations, although trends may also involve significant repulsive nonbonded interactions between the $R_2Si(R'_4C_5)(R''N)R'''$ ligation and the $H_3CB(C_6F_5)_3^-$ counteranion in the contact ion pairs. Thus, similar repulsive steric effects are expected in complexes **2b**−**d**, **f**, and **g**, which have similarly short Ti−C(2) distances. In the case of hydride **2e**, the smaller H ligand results in diminished interligand repulsive effects and, therefore, a contracted $Ti\cdots H_3C(2)B(C_6F_5)_3$ distance. The corresponding ion pair is, therefore, more stable, and the heterolytic ion pair separation process is correspondingly more endothermic. In the case of **2a** ($R' = CH_3$), the more sterically encumbered permethylated Cp ring induces greater repulsive interactions and an expanded Ti−C(2) bond length. The ion pair is, therefore, less stable, and the heterolysis process is correspondingly less endothermic.

In an additional analysis of ion pair heterolysis, the potential energy surface for the $H_2Si(C_5H_4)(t\text{-BuN})Ti(CH_3)\cdot H_3CB(C_6F_5)_3$ model complex was also investigated along the reaction coordinate for heterolytic ion pair dissociation. Figure 7 portrays the energies required for incremental $H_3CB(C_6F_5)_3^-$ displacement in the gas phase and in solution as a function of solvent dielectric constant. The energies were evaluated for selected Ti−$H_3CB(C_6F_5)_3$ bond distances while optimizing all other geometrical parameters without constraints. It can be seen that the energies increase substantially upon displacement of the $H_3CB(C_6F_5)_3^-$ ion from equilibrium; however, in the gas-phase, even considerable elongation (6 Å) of the $Ti\cdots H_3CB(C_6F_5)_3$ contact leaves residual stabilization energy ($\Delta E = -40$ kcal/mol) as compared to the case of noninteracting ion pairs (infinite separation; Figure 7). Note that this contact distance is nearly 3× longer than the equilibrium distance (2.435 Å). Thus, orbital overlap interactions are of minor relevance because the bonding is overwhelmingly electrostatic in character, while internal ion geometrical and electronic parameters closely approximate those of noninteracting, naked ionic species. Nevertheless, large residual Coulombic interactions are operative, despite the 6 Å separation, and the associated potential energy is approximately one-half of that required for infinite separation. Even further lengthening of the contact to 10 Å leaves a sizable (−30 kcal/mol) residual electrostatic interaction. This previously unappreciated electrostatic energy trend, of course, differs markedly from that which is found in classical homolytic covalent bond scissions where the energy for separations greater than 2× the equilibrium distance lies close to that for infinite separation.[18] The important catalytic consequence here is that the $Ti\cdots H_3CB(C_6F_5)_3$ contact can rather flexibly rearrange to greater ion pair separations for only a modest cost in energy (∼12 kcal/mol for an elongation of 1 Å from the equilibrium position). This observation provides a rationale for the $H_3CB(C_6F_5)_3^-$ group stereochemical mobility that is observed in dynamic NMR experiments,[1a,6] because the isotropically diffuse ionic bonding is described by a relatively flat potential surface.

Relative to the gas phase, the solvation medium strongly affects the energetics of incremental heterolytic ion pair separation (Figure 7). In less polar solvents such as benzene, the shape of the potential energy surface is similar to that for the gas phase in the <4 Å range. For greater distances, the curve is almost flat. Thus, solvation has a moderate influence for small (≤1.5 Å) displacements from equilibrium, whereas it strongly influences the potential surface for large distances. Note that in C_6H_6, the energy of noninteracting ion pairs is only 15 kcal/mol higher than that of the structure with a 10 Å contact. This is because residual Coulombic interactions in the same gas-phase structure are nearly counteracted in C_6H_6 by solvation. Upon further increasing the dielectric constant in C_6H_5Cl and CH_2Cl_2, other solvation patterns become evident. Again, the energetic trends approach the gas-phase behavior for $Ti\cdots H_3CB(C_6F_5)_3$ distances nearer to equilibrium (<4 Å), and sigmoidal patterns are observed with minima centered at ∼5Å (Figure 7). In addition, the ion pair structures with 10-Å Ti···C(2) separations are energetically comparable to the isolated, noninteracting ion pair. These data are in accord with solution-phase dynamic NMR results[6a,e] in which experimental barriers to unimolecular ion pair reorganization processes [eqs.(5, 6)] are significantly smaller than energies that were computed for total ion pair separation. These NMR results agree with the present findings because the very high barrier disfavors complete heterolytic dissociation/separation, while the observed ion pair reorganization behavior [eqs. (5),(6)] requires only more modest elongations coupled with repositioning of the counteranion from one side of the cation to the other, which is likely assisted by solvent molecule

(17) Lanza, G.; Fragalà, I. L. *J. Phys. Chem. A* **1998**, *102*, 7990.

(18) The presently adopted level of theory is inadequate to correctly describe the diffuse nature of the CH_3^- anion, and the computed EA of CH_3 is found to be endothermic.[18a,b] The EA of CH_3 that is quoted in Figure 9 (0.08 ± 0.03 eV) refers to the experimental value.[18c] (a) Sana, M.; Leroy G. *J. Mol. Struct.* (*THEOCHEM*) **1991**, *226*, 307. (b) Pople, J. A.; Schleyer, P. v. R.; Kaneti, J.; Spitznagel, G. W. *Chem. Phys. Lett.* **1988**, *145*, 359. (c) Drzaic, P. S.; Marks, J.; Brauman, J. I. In *Gas-Phase Ion Chemistry*; Bowers, M. T., Ed.; Academic Press: New York, 1984, Vol. 3, Chapter 21, p 167.

Table 7. Solvent Molecule Complexation Enthalpies $H_2Si(C_5H_4)(t\text{-BuN})TiCH_3^+ + solv \rightarrow H_2Si(C_5H_4)(t\text{-BuN})Ti(CH_3)(solv)^+ + \Delta H_{comp}$[a]

	HF	MP2	MP2/BSSE	
			gas phase	solvated ΔH_{comp}
$H_2Si(C_5H_4)(t\text{-BuN})TiCH_3\cdot(C_6H_6)^+$	−13 (−14)	−30 (−32)	−17 (−20)	−13 (−16)
$H_2Si(C_5H_4)(t\text{-BuN})TiCH_3\cdot(C_6H_5Cl)^+$	−16 (−14)	−23 (−24)	−15 (−16)	−5 (−8)
$H_2Si(C_5H_4)(t\text{-BuN})TiCH_3\cdot(CH_2Cl_2)^+$	−12 (−12)	−20 (−22)	−13 (−14)	−5 (−6)
$H_2Si(C_5H_4)(t\text{-BuN})TiCH_3\cdot(2\cdot CH_2Cl_2)^+$	only one solvent molecule is coordinated			

[a] Data in kcal/mol. Values in parentheses refer to calculations including polarization function.

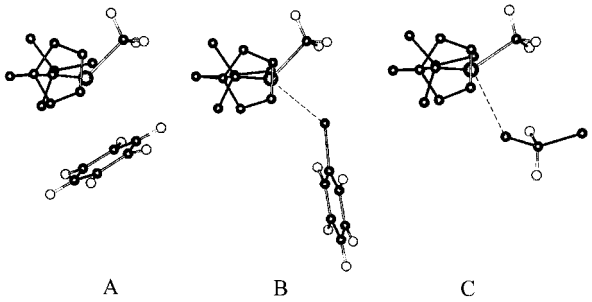

Figure 8. Molecular structures of naked cation−solvent molecule complexes: A, $H_2Si(C_5H_4)(t\text{-BuN})TiCH_3\cdot C_6H_6^+$; B, $H_2Si(C_5H_4)(t\text{-BuN})TiCH_3\cdot C_6H_5Cl^+$; and C, $H_2Si(C_5H_4)(t\text{-BuN})TiCH_3\cdot CH_2Cl_2^+$. Hydrogen atoms on the $H_2Si(C_5H_4)(t\text{-BuN})$ ligand have been omitted for clarity.

coordination in the transition state. A hypothetical transition state for this process is presented in **C**.

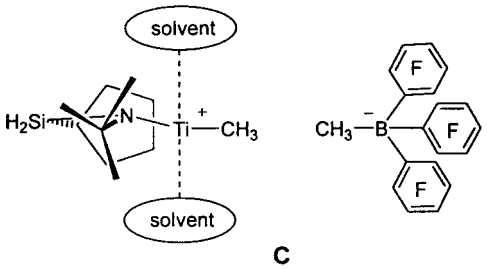

C

Energetics of Solvated Complexes. Naked $H_2Si(C_5H_4)(t\text{-BuN})TiCH_3^+$ cation structures stabilized by formation of discrete solvent coordination complexes were also investigated (eq 4). In the gas phase, coordination of a single solvent molecule is energetically favored (Table 7). Calculations including polarization functions for all of the three model systems invariably show slight shifts in the complexation energy even though different types of solvent ligation are present. Benzene is bound through the π system (η^3 coordination is found to be the most stable) with computed equilibrium Ti−C(C_6H_6) distances ranging from 2.81 to 4.12 Å. In contrast, C_6H_5Cl and CH_2Cl_2 are coordinated via a chlorine atom lone pair (Figure 8; Ti−Cl = 2.75 Å in both cases). The magnitudes of the computed gas-phase ΔH_{com} values for the present systems follow the trend $C_6H_6 < C_6H_5Cl < CH_2Cl_2$ (decreasing exothermicity) and reflect an electron donating capacity in the order $C_6H_6 > C_6H_5Cl > CH_2Cl_2$. Inclusion of nonspecific solvent effects results in greater stabilization of the naked cation relative to discrete cation−solvent coordination complexes, but with a net reduction in exothermicity that arises from specific complexation. The effects are largest for high-dielectric-constant solvents (C_6H_5Cl and CH_2Cl_2), with very weak complexation ($\Delta H_{comp} \approx -5$ kcal/mol), as compared to C_6H_6 (~ -13 kcal/mol). These results are in accord with experiment because the toluene complex $(CH_3)_2Si[(CH_3)_4C_5](t\text{-BuN})Zr(CH_3)\cdot(\text{toluene})^+B(C_6F_5)_4^-$ has been isolated, while similar complexes with C_6H_5Cl and CH_2Cl_2 have not been detected spectroscopically.[6e,g] The possibility of two CH_2Cl_2 solvent molecules coordinated to the $H_2Si(C_5H_4)(t\text{-BuN})TiCH_3^+$ cation was also investigated. No stable structure with both solvent molecules coordinated to the cation was found. All attempts resulted in strong coordination of one solvent molecule to the naked cation with a structure similar to that in Figure 8 C. The remaining solvent molecule is located far from the cation and slightly stabilizes it through van der Waals interactions (~1 kcal/mol).

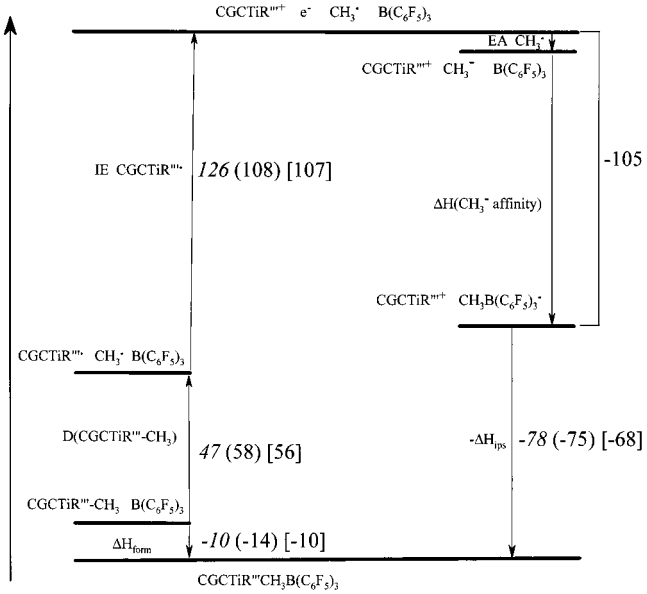

Figure 9. Thermodynamic cycle correlating the ion pair formation (eq 2) and heterolytic ion pair separation (eq 3) enthalpies. Values on the right of each step refer to: $H_2Si(C_5H_4)(t\text{-BuN})Ti(CH_3)_2$ (italics), $(CH_3)_2Si[(CH_3)_4C_5](t\text{-BuN})Ti(CH_3)_2$ (parentheses), and $H_2Si(C_5H_4)(t\text{-BuN})Ti[CH(CH_3)_2](CH_3)$ (brackets).

Specific single toluene solvent molecule−CGC cation complexation enthalpies have also been evaluated for $H_2Si(C_5H_4)(NH)TiCH_3^+$ at the DFT level.[5b] The computed values (−35.5 and −30.4 kcal/mol for gas-phase and solution, respectively) are somewhat higher than those presently reported (Table 7). This may be due to several factors, including (i) the simplified model cation used in the DFT calculations (substitution of the *t*-Bu group by H on the amido ligand) which allows stronger arene coordination, (ii) the different solvent molecule (toluene vs benzene) adopted, and (iii) possible overestimation of electron correlation.[10]

Thermochemistry of Ion Pair Formation and Separation

ΔH_{ips} and ΔH_{form} can be correlated to other molecular parameters in a thermodynamic cycle, as illustrated in Figure 9.[6a,d,e] The exothermic electron affinity of the $CH_3\cdot$ radical (EA $CH_3\cdot$) and borane methide affinity enthalpy (ΔH CH_3^- affinity) are invariant for a given Lewis acid, and in the present case, the sum is −105 kcal/mol.[18] It is evident that the ion pair binding energetics (an important parameter for the catalytic activity) are sensitive to the methide abstraction enthalpy, the homolytic bond

dissociation enthalpy [D(CGCTiR‴-CH_3)] and the ionization energy of the corresponding trivalent species (IE CGCTiR‴). The variation for two different CGC Ti complexes can be expressed by eq 7.

$$\Delta\Delta H_{ips} = \Delta H'_{ips} - \Delta H_{ips} = [D(Ti{-}CH_3) - D(Ti{-}CH_3')] + (IE\text{-}IE') - (\Delta H_{form} - \Delta H'_{form}) \quad (7)$$

Computation of the aforementioned molecular properties was performed for selected cases, in particular for $H_2Si(C_5H_4)$(*t*-BuN)Ti$(CH_3)_2$ (**1c**), $(CH_3)_2Si[(CH_3)_4C_5]$(*t*-BuN)Ti$(CH_3)_2$ (**1a**), and $H_2Si(C_5H_4)$(*t*-BuN)Ti[$CH(CH_3)_2$](CH_3) (**1g**); data are summarized in Figure 9. The most consistent variation, on passing from **1c** to **a** and **g**, is found in IE. This behavior is in accord with experimental ionization energy data for variously substituted biscyclopentadienyl Ti(III) complexes, $(R_nC_5)_2TiX$ (X = Cl, Br; R = H, CH_3),[19] which indicate a substantial reduction of the lowest IE (d^{-1} ionization) upon increasing cyclopentadienyl ligand methylation (~5 kcal/mol per methyl group for CpMe through Me_5Cp). Variations are also observed for the computed homolytic D(Ti(IV)−CH_3) bond dissociation energies, with greater values associated with the more heavily substituted precatalysts **1a**, and **g** vs **1c**. This trend reflects the reduced stability of Ti(III) species for electron-rich complexes **1a** and **g**. No experimental data are available for D(Ti−R) as a function of L for L_2TiR_2 species. However, experimental data for the average D(Zr−CH_3) bond dissociation energies in $(C_5H_5)_2Zr(CH_3)_2$ and $[(CH_3)_5C_5]_2Zr(CH_3)_2$ are essentially identical (67.2(1.0) and 67.0(1.0) kcal/mol, respectively).[20] The total energies of the ionization energy plus the homolytic dissociation processes then describe the strength of the Ti−CH_3 bond with respect to heterolytic dissociation in the various precatalysts (**1c** > **1a** > **1g**; 172, 165, and 160 kcal/mol, respectively) and, therefore, reflect the stability of the corresponding cations (**3c** < **3a** < **3g**). For **1c** and **g**, the computed methide abstraction enthalpies (ΔH_{form}) are identical, and therefore, the ΔH_{ips} variation depends on the balance between IE and D(Ti−CH_3). Analogously, in the case of **1a**, the higher stability of cation **3a** with respect to **3c** renders ΔH_{ips} less exothermic; however, a modest variation is found because of the greater exothermicity of ΔH_{form}.

Conclusions

The bonding and structural energetics of the species involved in olefin polymerization catalyst generation from CGC−Ti-based precatalysts activated by $B(C_6F_5)_3$ have been analyzed for the first time by ab initio formalisms. The calculated ion pair formation enthalpies (ΔH_{form}) depend both on the homolytic Ti−CH_3 bond enthalpy and on the ability of the alkide abstraction product to stabilize the resulting cationic center. These factors, in turn, are influenced by the electron donor and steric repulsive characteristics of the Ti, Si, Cp, and N substituents. Solvation slightly increases the exothermicity of the contact ion pair formation reaction (~3 kcal/mol) because of the greater stabilization of the ion-pair adduct via charge polarization. Nevertheless, modest variations are found when the solvent polarity (benzene, chlorobenzene and dichloromethane) is increased. There is generally good agreement between the calculated and experimental energetic and structural parameters.

The endothermicity of ion-pair separation (ΔH_{ips}) is diminished by the presence of electron-releasing groups on Cp, Si, and N, which reflects steric and electronic factors which stabilize the naked cation. The Ti σ-alkyl ligand has a similar effect on ΔH_{ips} because of stabilizing electronic, including agostic, interactions with the naked cation, as well as steric repulsions. Solvation strongly affects the position of this equilibrium because of the large stabilization of the charged $H_3CB(C_6F_5)_3^-$ and $R_2Si(R'_4C_5)(R''N)TiR'''^+$ species with respect to the contact ion pair. The presence of solvent also introduces greater flexibility in the $R_2Si(R'_4C_5)(R''N)TiR'''^+\cdots H_3CB(C_6F_5)_3^-$ bonding and significantly stabilizes this essentially electrostatic interaction at long Ti···C interatomic distances. This hetertofore unappreciated aspect of the bonding explains the experimentally established mobility of the $H_3CB(C_6F_5)_3^-$ group within the $R_2Si(C_5R'_4)(R''N)TiR'''^+$ coordination sphere and the facile displacement of $H_3CB(C_6F_5)_3^-$ simultaneous with solvent coordination and/or olefin activation/enchainment. ΔH_{ips} can be expressed as a function of ΔH_{form} and ionization energy of the related Ti(III) complex plus the homolytic Ti−CH_3 bond dissociation enthalpy. The resulting trends in ΔH_{ips} emphasize the capacity of the Ti ligation to stabilize the resulting cationic species.

Activation of the catalyst by the $B(C_6F_5)_3$ cocatalyst generally induces a ~0.3-Å abstractive displacement of a CH_3 group from the Ti center. However, variations are observed for **1a** (R′ = CH_3, R‴ = CH_3) and **1e** (R′ = H, R‴ = H) because of differing repulsive interactions between the Ti ligand array and the $B(C_6F_5)_3$ group. When the metal center passes from contact ion pair adducts to a naked Ti cation, it evolves from a pseudotetrahedral to pseudotrigonal coordination geometry, and the Ti−ligand bond lengths contract significantly, while the Ti-alkyl group assumes a conformation that electronically and sterically saturates the vacant metal coordination site.

Acknowledgment. This research was supported by the Ministero dell'Università e della Ricerca Scientifica e Tecnologica (MURST Rome), the Consiglio Nazionale delle Ricerche (Rome), and by the U.S. Department of Energy (grant 86ER13511).

JA000571R

(19) Vondrak, T.; Mach, K.; Varga, V. *Organometallics* **1992**, *11*, 2030.
(20) Schock, L. E.; Marks, T. J. *J. Am. Chem. Soc.* **1988**, *110*, 7701.